ACS Catalysis

Article

Mechanistic Insight to C–C Bond Formation and Predictive Models for Cascade Reactions among Alcohols on Ca- and Sr-Hydroxyapatites

Takahiko Moteki, and David W. Flaherty

ACS Catal., **Just Accepted Manuscript** • DOI: 10.1021/acscatal.6b00556 • Publication Date (Web): 04 May 2016

ACS Publications

ACS Catalysis is published by the American Chemical Society. 1155 Sixteenth Street N.W., Washington, DC 20036

Mechanistic Insight to C–C Bond Formation and Predictive Models for Cascade Reactions among Alcohols on Ca- and Sr-Hydroxyapatites

Takahiko Moteki[†,‡] and David W. Flaherty*[,†,‡]

[†]Department of Chemical and Biomolecular Engineering, University of Illinois Urbana-Champaign, Urbana, IL 61801

[‡]Energy Biosciences Institute, University of Illinois Urbana-Champaign, Urbana, IL 61801

*Corresponding Author

Phone: (217) 244-2816

Email: dwflhrty@illinois.edu

Abstract

Biomass-derived light alcohols (e.g., ethanol) may be upgraded via C–C bond formation to form larger alcohols and chemicals. The mechanism for coupling reactions among alcohols (i.e., Guerbet chemistry) is still debated, and the factors that determine the rates of subsequent, and inevitable, reactions among coupling products, and thus the product distributions, are not well understood. Here, the interpretation of the formation rates of products, *in situ* spectroscopy of surface intermediates, and evidence from isotope labeling experiments are combined to clarify the mechanism of the ethanol coupling over hydroxyapatite (HAP) catalysts. Initial C–C bonds are created by aldol condensation of acetaldehyde, derived *in situ* from ethanol, and involves a kinetically relevant deprotonation step to form the reactive enolate. *In situ* infrared spectra show that the coverage of ethanol-derived species far exceeds that of reactive aldehyde intermediates, which is consistent with C–C formation rates that inversely depend on ethanol pressure. Unsaturated aldehyde products are sequentially hydrogenated by the Meerwein–Ponndorf–Verley (MPV) reaction (i.e., C=O bond hydrogenation) and surface mediated H-transfer (i.e., C=C bond hydrogenation). The MPV reaction simultaneously supplies reactive acetaldehyde needed for the coupling reaction by dehydrogenating ethanol. Rate of self- and cross-coupling reactions among C_2–C_4 alcohols are similar as are the values of the apparent activation enthalpies, which shows that self- and cross-coupling rates depend weakly on the structure of the reactants on HAP catalysts, with few exceptions. The carbon number distribution of the products from ethanol coupling closely match predictions from an adapted step-growth model. Together, these findings show the mechanism for C-C bond formation between alcohol reactant on HAP catalysts and provide guidance for the production of higher carbon number species from alcohol coupling reactions.

Key words

alcohol coupling, hydroxyapatite, Guerbet reaction, step growth, Meerwein-Ponndorf-Verley, aldol condensation, cascade reaction

1. Introduction

Biomass has the potential to provide renewable and carbon neutral feedstocks for production of fuels and chemicals.[1-4] Many forms of biomass (e.g., sugarcane, corn, or straw) can be readily converted into ethanol, a platform chemical, by fermenting sugars (e.g., glucose, fructose, sucrose).[4-6] In turn, ethanol can be transformed to more valuable and higher carbon number (C_n) products by C–C bond formation reactions.[7-11] Reactive species derived from ethanol form 1-butanol, larger alcohols, and alkenes over heterogeneous catalysts that expose both acid and base sites (i.e., metal oxides,[12-15] mixed-metal oxides,[16-20] and hydroxyapatites[21-28]).[7,8] Both stoichiometric hydroxyapatite (HAP, $Ca_{10}(PO_4)_6(OH)_2$) and modified HAP have received a significant amount of attention for ethanol conversion,[7,8,21-29] because HAP produces 1-butanol with reasonable selectivity (~ 75%) at 10–15% conversion[22,23] and possesses acid and base properties that can be tuned by changing the identity of the metal (e.g., Ca or Sr) and the metal to phosphorous molar ratio (M/P) of the material.[21-24,30]

Following the formation of 1-butanol, C–C bond forming reactions continue and create heavier products ($C_{\geq 6}$).[21,22] The relative rates of self- and cross-condensation reactions determines the C_n and isomer distribution of the product,[22] and thus, their value for particular applications. For example, 1-butanol is desirable as a fuel additive, mid-chain (C_8–C_{12}) alcohols are useful for jet fuels, and predominately linear C_{12}–C_{18} alcohols can be used for diesel fuels.[31-33] Ideally, the selectivity towards a given category of alcohols would be high, because the fractionation of long-chain alcohols is energy intensive. Clarifying the network of reactions present during ethanol conversion to higher alcohols over heterogeneous catalysts would help to show how, and if, the product distribution may be controlled.

The details of the mechanism,[14,15,19,20,22-28] active intermediate,[20,24,29,34] and nature of the active sites[25,26,29,35-37] for forming the first C–C bonds between ethanol-derived intermediates on oxide catalysts is an active area of research, as summarized in recent reviews.[7,8] Yet, the mechanisms and networks of continuous secondary coupling reactions that produce $C_{\geq 6}$ products have received less attention. C–C bonds form over heterogeneous catalysts via one of three proposed pathways;[7,8] direct condensation between two alcohols,[15,27,28] condensation between aldehydes and alcohols,[14] or a more complex series of reactions that involve aldol condensation between aldehydes,[21-26] and the relative contributions of these pathways likely depend on both the reaction conditions and the identity of the catalyst. The latter pathway consists of a sequence of steps that is thought to include dehydrogenation of alcohols to aldehydes, aldol addition of two aldehydes, dehydration of the aldol, and subsequent hydrogenation steps to form aldehydes or alcohols.[7,8,38] Insight into the factors that ultimately determine the C_n and structural distributions of $C_{\geq 6}$ product alcohols requires that we understand also the mechanism for C–C bond formation between alcohol derivatives and the identity of the reactive species that participate in each elementary step.

Here, we describe the network of reactions that convert ethanol into C_4–C_{12} alcohols and aldehydes over Ca- and Sr-HAP, and show how the rates of the parallel coupling pathways depend on intrinsic properties of the reactive intermediates and the catalytic surfaces. Comparisons of reaction rates for C–C bond formation measured as functions of ethanol (1.2–6.2 kPa), acetaldehyde (0.07–0.26 kPa), and hydrogen (20–100 kPa) pressures implicate acetaldehyde as a reactive intermediate. C–C bonds form by steps involving kinetically relevant deprotonation of acetaldehyde and subsequent aldol condensation. Isotope labeling experiments show that direct H-atom transfer between ethanol and formed aldehydes via the Meerwein-

Ponndorf-Verley (MPV) reaction concurrently saturates C=O bonds to form heavier alcohols and produces acetaldehyde, however, surface mediated H-atom transfer pathways hydrogenate C=C bonds. Independent rate measurements for self-coupling reactions of C_2, C_3, and C_4 alcohols as a function of reactant conversion (0–10%) show that pseudo-first order rate constants vary only by a factor of two between ethanol and larger alcohols. In addition, rate ratios for cross-coupling reaction pathways that involve the deprotonation of either C_2 or C_4 aldehydes to form either 1-hexanol or 2-ethyl-butanol, respectively, remain constant and close to unity (~ 0.8) from 548-598 K. These results, and expectations that further increases in alcohol chain length will have diminishing effects on reactivity, suggest that apparent rate constants and activation enthalpies for all simultaneous self- and cross-coupling pathways are similar. Moreover, measurements of ethanol consumption rates and quantitative analysis of product distributions among C_4-C_{12} alcohols show that the reaction network of all condensation pathways match predictions of an adapted step-growth polymerization model.[39,40] The degree of branching in these species increases monotonically with conversion, because reactions between two $C_{>2}$ aldehydes create products with one more ^{3}C-atom than the reactants. Overall, these findings show that a simple model provides useful predictions for several properties of the final product distribution. However, this also indicates that such reaction networks are not suitable for selectively creating product alcohols with narrow distributions of C_n or branching characteristics.

2. Materials and Methods

2.1. Preparation of Ca- and Sr-HAP Catalysts

The Ca-HAP catalyst with a Ca/P ratio of 1.67 was purchased from Acros Organics (Lot: A0333466), while other Ca- and Sr-HAP catalysts with different metal to phosphorous ratios (M/P) were prepared by precipitation methods described previously.[21-24,30] Briefly, Ca- and Sr-HAP catalysts were prepared from solutions created by combining deionized water (17.8 MΩ) with $(NH_4)_2HPO_4$ (Sigma-Aldrich, 99.0%) and either $Ca(NO_3)_2{\cdot}4H_2O$ (Sigma-Aldrich, 99.0%) or $Sr(NO_3)_2$ (Sigma-Aldrich, 99.0%). The M/P of the resulting catalysts were controlled over the range of 1.61–1.74 by changing the ratio of the metal and phosphorous precursors in the synthesis solutions. Specifically, 300 cm^3 of an aqueous solution containing either $Ca(NO_3)_2{\cdot}4H_2O$ or $Sr(NO_3)_2$ at a concentration of 0.667–0.8 M was added to 300 cm^3 of aqueous 0.4 M $(NH_4)_2HPO_4$. Aqueous NH_4OH (28–30% as NH_3, Macron Fine Chemicals) was added to the solution to achieve an initial pH of 10. The mixed synthesis solution was then heated to 353 K and stirred for 12 h to complete the precipitation of the HAP product. The precipitated products were filtered and washed with 1 L of deionized water. Subsequently, the recovered sample was dried in a stagnant air at 373 K for 12 h in a preheated oven. The dried powders were pelletized, crushed, and sieved to obtain HAP agglomerations with diameters of 230–560 μm.

2.2. Characterization of HAP Materials

Powder X-ray diffraction (XRD) patterns were collected on a Siemens Bruker D5000 using CuKα radiation (λ = 0.1542 nm, 40 kV, 30 mA) between 5° and 60° (2θ) with 0.05° steps and a scanning speed of 2° min^{-1}. The XRD patterns of all five materials are shown in the Supporting Information (Figure S1) and all detected peaks match only those for the known structure of hydroxyapatite (Table 1), which confirms that only Ca- and Sr-HAPs phases formed without structural impurities, such as brushite.[30] Scanning electron microscope (SEM) images were obtained on a Hitachi S4700 with an accelerating voltage of 3–10 keV. Prior to SEM

measurements, the samples were lightly sputtered with Pt/Au in an Ar atmosphere (EMITECH K575). The morphologies of the HAP samples were spherical and rod-like for Ca- and Sr-HAP samples, respectively (Figure S2). These morphologies differ from the plate-like Ca-HAP synthesized in solutions with pH values of 9 or less,[21,22,30] and this indicates that our synthesis directly forms HAP due to the higher pH value of 10 and does not involve an intermediate brushite structure.[30] The specific surface area of each sample was determined using a single point N_2 adsorption measurement at 77.3 K at a relative pressure (P/P_0) of 0.31 by Micrometrics. Prior to N_2 adsorption, the HAP samples were degassed at 673 K in vacuum for 4 h. These physisorption measurements show that the synthesized Ca- and Sr-HAP materials possess specific surface areas of 60–70 and 35–40 m^2g^{-1}, respectively (Table 1).

The chemical composition of each sample was measured by inductively coupled plasma-mass spectrometry (ICP-MS; PerkinElmer, ELAN DRC-e) to determine the bulk molar ratios of Ca to P (Ca/P) and Sr to P (Sr/P). All samples fell within the range of M/P values of (1.61–1.74), and bulk M/P values changed monotonically with that of the synthesis solution. It should be noted that the M/P ratio of surface is correlated with, but not equal to, that of bulk.[22] Additional measurements are, however, necessary to determine how the chemical function and number of base sites on the HAP surface change with M/P ratios and metal identity.[30,36] Therefore, the number and functional strength of base sites on HAP surfaces was determined by temperature-programmed desorption (TPD) spectra of CO_2 using a custom-made system equipped with a quadrupole mass spectrometer (ThermoStar, Pfeiffer). During TPD measurements, 0.1 g of HAP was loaded into a tubular glass reactor and heated at 5 K min^{-1} to 773 K in flowing He (25 cm^3 min^{-1}, SJ Smith, Ultra High Purity) and held at 773 K for 1 h, with the intent to desorb all H_2O and other impurities adsorbed on the surface. Subsequently, the sample was cooled to 323 K in

stagnant He, after which, the catalyst was exposed to a flowing stream of 50 % CO_2/He (50 cm^3 min^{-1}, SJ Smith, 99.995%) for 1 h to saturate the surface with CO_2. Next the reactor and catalyst bed was flushed with He (25 cm^3 min^{-1}) for 3 h at 323 K to remove weakly adsorbed CO_2. The TPD spectra was then obtained by heating the sample at a rate of 5 K min^{-1} to 873 K in a 25 cm^3 min^{-1} He flow while monitoring mass-to-charge ratios of 44, 18, and 4 using the mass spectrometer to detect the partial pressures of CO_2, H_2O, and He respectively. The absolute amount of CO_2 that desorbed from each sample was calculated using the known flow rate of the system and the calibrated sensitivity of the mass spectrometer for CO_2. The resulting CO_2 TPD spectra (Figure S3) show distinct desorption peaks at ~360 K and ~420 K on Ca-HAP, which correspond to distinct adsorption sites that can be qualitatively described as weaker and stronger base sites, respectively. The integrals of the TPD peaks increase with increasing M/P ratios, which suggest that HAP catalysts with higher M/P ratio have a larger number of surface base sites. These results are consistent with expectations that larger Ca content will result in the increase of base sites,[21-23,30] possibly OH^- and O^{2-} moieties.[35,36]

2.3. *In Situ* Transmission Fourier Transform Infrared Spectroscopy

The identity and coverage of surface intermediates formed during ethanol coupling reactions on HAP catalysts was probed using *in situ* transmission Fourier transform infrared (FTIR) spectroscopy using a custom-made transmission cell, described previously.[41] Catalyst wafers (50–100 mg) were pressed into a self-supporting wafer and placed within the stainless-steel cell equipped with CaF_2 windows and connected to a gas manifold, which enabled thermal treatments and adsorption-desorption experiments to be carried out *in situ*. The temperature of the cell was controlled with a custom-made metal heating assembly,[41] and the temperature of the wafer was measured with a K-type thermocouple located within the cell. Ethanol was fed via a syringe

pump (Legato 100, KD Scientific) and was vaporized inside the gas transfer lines, which were heated to 323 K using electrical heating tape. Wafers were first pretreated at 673 K for 1 h under helium flow (100 cm^3 min^{-1}), then cooled to 573 K prior to introducing ethanol (4.6 kPa C_2H_5OH, 96 kPa H_2, Ca/P =1.67). In order to minimize the spectral contributions from aromatic surface residues that form during the reaction, the ethanol flow was stopped after 30 min and the cell was flushed with He prior to taking a background scan. Ethanol was then re-introduced into the cell and the *in situ* sample spectra were obtained after waiting 30 min for the system to reach steady-state. Spectra were recorded by the spectrometer (Bruker, TENSOR 37), and each spectra was co-added from 32 scans obtained at a resolution of 4 cm^{-1}.

2.4. Steady-State Catalytic C–C Bond Formation and 1-Butanol Formation Rates and Product Selectivities

Alcohol coupling reactions were carried out using a U-shaped, tubular glass reactor with a packed-bed configuration. The reactor was placed in a vertically-aligned temperature-controlled tubular furnace (National Element, Inc., FA-120). The temperature of the catalyst bed was measured with a K-type thermocouple coaxially-aligned with the glass reactor and in direct contact with the catalyst bed (0.05–0.2 g) and was controlled by a PID controller (WATLOW, EZ-ZONE) connected to a variable transformer. The HAP catalysts were treated *in situ* by heating at 10 K min^{-1} to 773 K and holding for 2 h under He flow (20 cm^3 min^{-1}) to remove adsorbed water and other molecules (e.g., CO_2) before measuring catalytic rates. Flow rates of He (SJ Smith, Ultra High Purity) and H_2 (SJ Smith, 99.999%) were set by mass flow controllers (MFC, 601 series, Porter). Liquid phase reactants (ethanol, Decon's Pure Ethanol 200 Proof, 100%; acetaldehyde, Fluka, 99.5%; 1-propanol, Fisher Scientific, certified grade; 1-butanol, Fisher Scientific, 99.9%; and crotonaldehyde, Aldrich, 99%, predominantly trans) were fed via a

syringe pump (Legato 110, KD Scientific) and were vaporized inside the 1/4" stainless steel transfer lines, which were heated to > 473 K using electrical heating tape. Volatile reactants (e.g., acetaldehyde) were fed as 10–30 vol % mixture in ethanol. The flow rates of all reactants were varied in order to control both the partial pressure and surface residence time of the reactants during experiments. The total pressure of the system was maintained at 101 kPa by co-feeding H_2 with the other reactants as needed. H_2 gas was used as a carrier gas instead of conventional inert gas (i.e., He) to maintain higher C-C bond formation rates, because H_2 slows the rate of carbon deposition on the catalyst as shown by comparisons between carbon balances and thermogravimetric analysis of spent catalysts (Figure S4). Before measuring the change in C-C bond formation rates as a function of reactant pressures or temperature, the system was allowed to reach steady-state at 5 kPa ethanol and 96 kPa H_2, which took approximately 6-8 hours (Figure S4a).

The identity and concentrations of reactants and products in the reactor effluent stream were measured using a gas-chromatograph (GC, 6850, Agilent) equipped with a capillary column (DB-WAX, 30 m × 0.25 mm × 0.25 μm) and a flame ionization detector (FID). The retention time for each component was determined using standard chemicals (Sigma-Aldrich, C_2–C_8 *n*-alcohols and C_2–C_4 *n*-aldehydes), and the molecular speciation of these and heavier products was confirmed using a gas-chromatograph mass-spectrometer (GC-MS, QP2010 Ultra, Shimadzu). Rates were measured at <15% conversion of the limiting reactant to identify primary reactions and to ensure that depletion of reactants across the bed had a minimal influence on measured rates. Mass-averaged rates for each reaction pathway are calculated as a number of the reaction event per unit time normalized by the initial moles of reactants and the weight of catalyst. The number of the C–C bond formation events is calculated by multiplying the moles of formed C_{2i}

species ($i \geq 2$) by i-1. For example, C_6, C_8, and larger C_{2i} products are formed using 2, 3, and $i-1$ ethanol molecules, respectively. C–C bond formation rates are reported as a number of C–C bond formation event per second per grams of catalyst ((mole) (g catalyst s)$^{-1}$). Selectivities are reported based on moles of carbon of the products (C-%). Measured rates were corrected to account for catalyst deactivation by measuring rates at a standard set of conditions multiple times within each experiment. After initial rapid deactivation over a period of 6 hours, the C-C bond formation rates decrease slowly over time (Figure S4a). The change in the number of active sites as a function of time on stream was determined by linear interpolation of relative site counts estimated from rates measured every 10–12 hours at identical conditions.

2.5. Catalytic Hydrogenation of Butyraldehyde, Crotyl Alcohol, and Crotonaldehyde to 1-Butanol

Hydrogenation reactions of butyraldehyde, crotyl alcohol, and crotonaldehyde were carried out using the reactor and pretreatment protocols used to study C–C bond formation reactions (section 2.4). The liquid phase reactants (2-propanol-d_8, Aldrich, 99.5 atom % D; butyraldehyde, Fluka, 99.0%; crotyl alcohol, Aldrich, 96%, mixture of cis and trans; crotonaldehyde, Aldrich, 99%, predominantly trans) were fed into flowing H_2 within reactor using a syringe pump. 2-Propanol-d_8 was fed to the reactor in a 20 mol % mixture in *tert*-butanol (Fischer Scientific, certified grade). The reactor effluent was collected by bubbling through an ethanol solution at the outlet of the reactor, and the mass spectra of all product species were collected using a gas-chromatograph mass-spectrometer (GC-MS, QP2010 Ultra, Shimadzu). The shift in the mass spectrum of the 1-butanol obtained by catalytic reaction with the mixture of 2-propanol-d_8 and *tert*-butanol was compared with that of purely hydrogen containing 1-butanol and crotyl alcohol.

3. Results and Discussion

3.1.1. Evidence for Aldehyde as Reactive Intermediates

Figure 1a shows that the steady-state C–C bond formation rate (r_{C-C})[42] on Ca-HAP is approximately 0.1 μmol g_{catal}^{-1} s^{-1} (4.8 kPa C_2H_5OH, 96 kPa H_2, 1.67 Ca/P, 548 K), and r_{C-C} increases by more than an order of magnitude when 0.26 kPa C_2H_4O is co-fed to the reactor. This significant change suggests that acetaldehyde is an active intermediate in C–C bond formation, which produces C_4 and larger enals, aldehydes, and alcohols. The products contain a broad distribution of species (Table 2), which at 8.2% conversion include C_4 alcohols and aldehydes (~86 C-%, 1-butanol, butyraldehyde, crotyl alcohol, and crotonaldehyde), C_6–C_8 alcohols and aldehydes (~8 C-%), C_2–C_6 alkenes (~4 C-%), and other species (~2 C-%) when only ethanol is fed to the reactor (4.8 kPa C_2H_5OH, 96 kPa H_2, 1.67 Ca/P, 548 K). The C_4 products predominantly consist of 1-butanol and crotyl alcohol while crotonaldehyde and butyraldehyde are present only in trace quantities (Table 2), which suggests that surface reaction pathways hydrogenate C=O bonds more readily than C=C bonds. The large number of products shows that the system involves a complex sequence of intermediate steps that form C–C bonds. The significant fraction of $C_{\geq 6}$ products suggest that these reactions occur in cascades that add significant amounts of C_2-intermediates to primary and secondary products even at low conversions (<10%) of acetaldehyde and ethanol. Figure 1b shows the product selectivities for C_4 products as a function of the total C_2 conversion at higher acetaldehyde and lower ethanol pressures (1 kPa C_2H_5OH, 0.35 kPa C_2H_4O, 100 kPa H_2, 1.67 Ca/P, 548 K). Selectivities extrapolated to zero conversion show that crotonaldehyde, which is the product from the aldol

condensation of acetaldehyde, is the sole primary product and that more saturated C_4 species (e.g., butyraldehyde, crotyl alcohol, and 1-butanol) form as secondary products following hydrogenation. These results (Figure 1 and Table 2) strongly suggest that C–C bond formation occurs by aldol condensation of two acetaldehyde molecules over stoichiometric Ca-HAP catalyst at these conditions. Moreover, the change in product selectivities with conversion (Figure 1b) are not consistent with other mechanisms proposed such as direct condensation between two ethanol molecules[15,27,28] or between ethanol and acetaldehyde,[14,15,26] because such mechanisms are reported to produce 1-butanol, butyraldehyde, and crotyl alcohol as primary products. The elementary steps and mechanism for C-C bond formation on HAP are further described below.

3.1.2. C–C Bond Formation and Hydrogenation

Figure 2 shows that C–C bond formation rates increase in proportion to the acetaldehyde pressure (Figure 2a, $r_{C-C} \sim [C_2H_4O]^{1.0}$; 4.8 kPa C_2H_5OH, 96 kPa H_2), decrease with the ethanol pressure (Figure 2a, $r_{C-C} \sim [C_2H_5OH]^{-0.3\pm0.2}$; 0.1 kPa C_2H_4O, 96 kPa H_2), and do not depend on the hydrogen pressure (Figure 2b, $r_{C-C} \sim [H_2]^0$; 5 kPa C_2H_5OH) over Ca-HAP (1.67 Ca/P, 548 K). These observations (Figure 2) are consistent with previous measurements, suggesting a kinetically-relevant step that involves a reaction of acetaldehyde and active site inhibition by ethanol.[23,26] Neither gaseous H_2 or surface intermediates derived from H_2 (i.e., chemisorbed H-atoms (H*)) appear to play a role in any kinetically relevant steps that couple acetaldehyde surface intermediates.[23,24]

The products contain high ratios of alcohols to aldehydes for each carbon backbone observed (Table 2), which suggests that rapid hydrogen transfer saturates unsaturated products (e.g., crotonaldehyde) prior to their desorption from HAP surfaces. Hydrogen transfer between alcohols and aldehydes on oxide surfaces may occur by one of two mechanisms[7,8,43] which include direct intermolecular hydride transfer, also known as the Meerwein–Ponndorf–Verley (MPV) reaction (Scheme S1a)[23,26,44] or surface mediated hydrogenation (Scheme S1b).[20] Surface mediated hydrogenation, which is common on metals,[20] involves activation and transfer of H-atoms from both gas phase H_2 and alcohols. However, our results (Figure 2b) and others[23,24] show that gaseous H_2 has no effect on reaction rates or product selectivity, which suggest that H_2 is not an effective H-atom donor during reactions on HAP surfaces. Recent reports have suggested that aldol condensation products (e.g., crotonaldehyde, butyraldehyde) hydrogenate by H-atom transfer from surface ethanol molecules following the MPV mechanism over HAP,[7,8,23,26] yet have not provided direct evidence for this pathway. It is difficult to determine whether hydrogen transfer occurs by surface mediated routes or by the MPV mechanism using rate measurements alone, however, isotope labeling techniques[45] can differentiate between these pathways.

Figure 3 shows the mass spectrum of 1-butanol formed after hydrogenation of butyraldehyde or crotyl alcohol with a mixture of 2-propanol-d_8 and *tert*-butanol (0.5 kPa C_4H_8O or C_4H_7OH, 0.6 kPa C_3D_7OD, 2.4 kPa *tert*-C_4H_9OH, 97 kPa H_2, 1.67 Ca/P, 573 K). Under these conditions with the excess of *tert*-butanol, the HAP surface mediates fast H/D exchange between the –OD and –OH groups in the alcohols (2-propanol-d_8 and *tert*-butanol, respectively), which causes the majority of the 2-propanol molecules to become the C_3D_7OH isotopologue. The ratio of H- to D-atoms on the Ca-HAP surface is assumed to be approximately four, because the zero point

energy differences between the O-H and O-D bonds in the organic reactants and those between the O-H and O-D bonds of surface hydroxyls are similar[46] and consequently these H- to D-atom ratio should match that of –OH to –OD groups in the reactant mixture of perhydrogenated *tert*-butanol (2.4 kPa) and perdeuterated 2-propanol (0.6 kPa). Figure 3a shows that the 1-butanol produced by hydrogenating butyraldehyde (Figure 3a, red) has a molecular weight 1 amu greater orthan that of perhydrogenated 1-butanol (C_4H_9OH, Figure 3a, black), and this comparison suggests that 2-propanol-d_7 ($CD_3CDOHCD_3$) formed *in situ* acts as the hydrogen donor and directly transfers the β-D and the α-H to the C-atom and the O-atoms, respectively, of the C=O group in butyraldehyde to produce C_4H_8DOH by the MPV reaction (Scheme S1a). If hydrogen transfer occurred by the surface mediated process (Scheme S1b), butyraldehyde would be hydrogenated with surface H/D-atoms, among which the majority are H*-atoms under these conditions (2.4 kPa *tert*-C_4H_9OH, 0.6 kPa C_3D_7OD). Consequently, the product 1-butanol would be primarily perhydrogenated and would have a mass spectrum indistinguishable from that for C_4H_9OH. On the other hand, Figure 3b shows that the 1-butanol produced by hydrogenating crotyl alcohol (Figure 3b, blue) has a mass spectrum almost identical to that of perhydrogenated 1-butanol (Figure 3b, black), which shows that C=C bond hydrogenation proceeds via surface mediated H-atom transfer (Scheme S1b). The comparisons between the spectra (Figure 3) would give compelling evidence that, within this reaction network, the hydrogenation of C=O bonds occurs by H-transfer from alcohol reactants via the MPV reaction mechanism, which is broadly thought to transfer H-atoms in a concerted manner.[43] These data, however, would be consistent also with a sequential transfer of H-atoms such as direct H-atom transfer from the α-carbon of the surface alkoxide to that of the aldehyde via a MPV-*like* intermediate[44] and subsequent H-atom transfer to the O-atoms of the aldehyde via a surface mediated pathway. On the other hand,

hydrogenation of C=C bonds occurs by transfer of two H-atoms formed on the catalyst surface via surface mediated hydrogenation. Isomerization reaction between butyraldehyde and crotyl alcohol are much slower than these hydrogenation reactions, because we observed nearly perfect 1 or 0 amu MS shifts suggesting that each hydrogenation pathway does not contribute simultaneously.

These findings are consistent also with the outcome of similar isotope labeling experiments that probed pathways for H-transfer to crotonaldehyde. The hydrogenation of crotonaldehyde to crotyl alcohol and that of crotonaldehyde to 1-butanol (Figure S5) both show a 1 amu shift relative to the perhydrogenated products. These results, together with those for hydrogenation of butyraldehyde (Figure 3a) and crotyl alcohol (Figure 3b), suggest that among all unsaturated species in this system, the MPV reactions is the predominant mechanism to hydrogenate C=O bonds and surface mediated H-transfer hydrogenates C=C bonds. In addition, the high ratios of alcohols to aldehydes (i.e., $[C_4H_9OH]/[C_4H_8O] > 100$; $[C_4H_7OH]/[C_4H_6O] > 10$) for each carbon backbone observed (Table 2) suggests that the MPV reaction (i.e., C=O bonds hydrogenation) occurs more readily than surface mediated hydrogenation (C=C bonds hydrogenation). These observations strongly suggest that enals formed by aldol condensation reactions first form unsaturated alcohols by the MPV reaction and subsequently hydrogenate to form alcohols by surface mediated H-transfer. At steady-state, the MPV process also dehydrogenates ethanol to form acetaldehyde, which is the active intermediate for C–C bond formation, as discussed in the following section.

3.1.3. Elementary Steps and Rate Equation of Initial Ethanol Coupling Reaction

Scheme 1 shows a sequence of elementary steps that accurately describes the effects of acetaldehyde, ethanol, and hydrogen pressures on C–C bond formation rates (Figure 2) and accounts for H-atom transfer between alcohol and aldehyde species by the MPV mechanism on HAP catalysts (Figure 3). These steps involve Lewis acid sites ($*_A$; Ca- or Sr-atoms) and base sites ($*_B$; O- or OH-moieties) that are known to exist on HAP surfaces based on FTIR studies[26,35,36] and the absence of spectral features indicative of Brønsted acid sites (i.e., formation of pyridinium ions upon adsorption of pyridine).[37,47]

Scheme 1 includes ethanol adsorption on acid sites (1.1) and dehydrogenation to form ethoxide (1.2),[29,48,49] and then further dehydrogenation to form acetaldehyde (1.3). Acetaldehyde may desorb (1.4) or deprotonate at the α-carbon to the carbonyl by reaction with an adjacent base site to form a carbanion (i.e., enolate) (1.5). The enolate undergoes nucleophilic attack onto an acetaldehyde molecule bound at a vicinal acid site to form a C–C bond (1.6). An aldol forms by subsequent protonation (1.7) and dehydrates to form the unsaturated aldehyde (i.e., crotonaldehyde) (1.8). Crotonaldehyde may hydrogenate to form crotyl alcohol by the MPV reaction (1.9), and then hydrogenate further by surface mediated H-transfer to form 1-butanol (1.10). All C_4 products (i.e., crotonaldehyde, crotyl alcohol, and 1-butanol) may desorb in reversible steps (1.11–1.13). Concomitantly, the MPV reaction that transfers hydrogen from ethanol to crotonaldehyde also produces acetaldehyde needed for the reaction (1.9). Finally, H-atoms bound to base sites may recombinatively desorb to form H_2 (1.14).[7,8] Adsorption of ethanol (1.1), desorption of acetaldehyde (1.4), and desorption of C_4 alcohols (1.12–1.13) are assumed to be quasi-equilibrated (QE), whereas deprotonation of the aldehyde (1.5) to form the carbanion is kinetically relevant.[26] Step (1.14) is not quasi-equilibrated and further the rate of

formation of surface H-atoms by dissociative adsorption of gas phase H_2 must be slow, because C–C bond formation rates do not depend on the H_2 pressure (Figure 2b).

Following Scheme 1, C–C bond formation rates are proportional to the number of adsorbed aldehydes ($[C_2H_4O*_A]$) and the probability of finding an unoccupied, adjacent base site ($[*_B]$):

$$r_{C-C} = k_5 \frac{[C_2H_4O*_A]\cdot[*_B]}{[L_B]} \qquad (1)$$

Here, k_5 is the rate constant for deprotonating acetaldehyde, and $[C_2H_4O*_A]$, $[*_B]$, $[L_B]$ are the numbers of acetaldehyde surface intermediates, unoccupied base sites, and the total number of reactive base sites, respectively. It should be noted that the number of base sites, $[L_B]$, also reflect the number of acid sites, $[L_A]$, because the acid and base sites in Eq. (1) should be an adjacent pair (see supporting information for further details) as proposed in the previous literature, in which CaO/PO_4^{3-} pairs is shown to catalyze the aldol condensation.[26] Equation 1 takes a new form after accounting for quasi-equilibrated (QE) acetaldehyde desorption (Scheme 1, step 1.4).

$$r_{C-C} = k_5 K_4 \frac{[C_2H_4O]\cdot[*_A]\cdot[*_B]}{[L_B]} \qquad (2)$$

Here, K_4 is the equilibrium constant for desorption of acetaldehyde (Scheme 1, steps 1.4), $[C_2H_4O]$ is the gas-phase concentration of acetaldehyde, and $[*_A]$ is the number of unoccupied acid sites. The total numbers of available acid sites ($[L_A]$) and those of base sites ($[L_B]$) are equal to the sum of all likely surface intermediates at each site:

$$[L_A] = [*_A] + \sum_1^n [C_{2,i} *_A] + \sum_1^m [C_{4,i} *_A] \qquad (3)$$

$$[L_B] = [*_B] + [H *_B] \qquad (4)$$

where $\sum_1^n[C_{2,i}*_A]$ and $\sum_1^m[C_{4,i}*_A]$ represent the total number of all possible C_2 (e.g., ethanol, ethoxide, acetaldehyde) and C_4 (e.g., 1-butanol, butyraldehyde, etc.) surface species, respectively, and $[H*_B]$ is the number of H-atoms on base sites. The number of $C_{\geq 6}$ oxygenates and other species (e.g., alkanes and ethers) are assumed to be much smaller than C_2–C_4 intermediates, and therefore negligible, because the concentrations of C_4 products are much higher than that of $C_{\geq 6}$ products or side products (Table 2). The combination of Eqs. (2–4) gives the following rate expression for C–C bond formation:

$$\frac{r_{C-C}}{[L_A]} = k_5 K_4 \frac{[C_2H_4O]\cdot[*_A]\cdot[*_B]}{([*_A]+K_i\sum_1^n[C_{2,i}]+K_i\sum_1^m[C_{4,i}])([*_B]+[H*_B])} \qquad (5)$$

Measured C–C bond formation rates show a linear dependence on acetaldehyde (Figure 2a) and negative dependence on ethanol ($r_{C-C} \sim [C_2H_5OH]^{-0.3\pm0.2}$; Figure 2a), which is consistent with Eq. (5) when ethanol-derived species occupy a significant fraction of the acid sites. Thus, the mechanistic interpretation of C–C bond formation rates imply that surface species derived from gaseous ethanol (e.g., ethoxide or ethanol) are among the most abundant reactive intermediates (MARI) on acid sites. The identity of these species was determined by analysis of *in situ* FTIR spectra, described below.

Figure 4 shows *in situ* FTIR spectra (3100–1500 cm^{-1} region) of the surface species that form on Ca-HAP under ethanol flow (5 kPa C_2H_5OH, 96 kPa H_2, 573 K, 1.67 Ca/P). Figure 4a spectra of the surface species that form feeding ethanol for 2 – 50 minutes, and a control measurement taken under same condition with an empty cell (Figure 4a, bottom) shows that the IR absorption features from gas-phase species are negligible. Absorption features at 3000–2800 and 1600–1500 cm^{-1} correspond to alkane ν(C–H) and aromatic ν(C=C) modes, respectively.[50] A complete absence of features between 1800–1600 cm^{-1} indicates that the number of carbonyl groups

among the surface species is negligible, and therefore, that the surface coverage of aldehydes is insignificant. Removal of ethanol from the inlet to the FTIR cell causes the intensity of the features at 3000–2800 cm^{-1} region to drop by more than 50% within 100 seconds, however, the intensity of the features at 1600–1500 cm^{-1} remain constant (Figure S6), which suggests that both weakly adsorbed reactive species and strongly adsorbed aromatic species coexist on the surface. Figure 4b shows a spectrum of only the reactive surface intermediates obtained by subtracting a spectrum taken of a used catalyst after removing ethanol from the feed. The main four bands at 2972, 2934, 2905, and 2877 cm^{-1} (Figure 4b) are attributed to the $\nu_{as}(CH_3)$, $\nu_{as}(CH_2)$, $\nu_s(CH_3)$, and $\nu_s(CH_2)$ modes, respectively, of adsorbed ethanol (or ethoxide) on Ca-HAP.[29,48,49] Together these observations (Figures 4 and S6) suggest that absorbed ethanol (or ethoxide) are a MARI on acid sites. This conclusion is consistent with steady-state isotopic transient kinetic analysis (SSITKA) by Davis, which showed that the number of surface intermediates on Ca-HAP that desorb to form ethanol (5 μmol m^{-2}) is larger than those that form 1-butanol (1.1 μmol m^{-2}) and much larger than those that form acetaldehyde (0.082 μmol m^{-2}) at operating conditions (8.1 kPa C_2H_5OH, 123 kPa He, 613 K, 75 cm^3 min^{-1})[29] similar to those used here.

These results, together with the negative dependence of C–C bond formation rates on ethanol pressure (Figure 2a), suggest that ethanol inhibits C–C bond formation by displacing acetaldehyde from the pairs of neighboring acid and base sites (e.g., adjacent CaO and PO_4^{3-} moieties)[26] needed for kinetically relevant acetaldehyde deprotonation (Scheme 1, step 1.5)." Surface H-atoms will be also formed via O–H rapture of adsorbed ethanol along with ethoxide formation (Scheme 1, step 1.2), and these species will increase with the pressure of ethanol.

Therefore, even if this step is ineligible in Eq.5, both will contribute to the inverse dependence of C–C bond formation rates on ethanol pressure.

Collectively, these assumptions regarding surface coverages cause Eq. 5 to take the form:

$$\frac{r_{C-C}}{[L_A]} = k_5 K_4 \frac{[C_2H_4O]}{1+K_1[C_2H_5OH]} \qquad (6)$$

which is consistent with the measured dependencies of r_{C-C} on reactant pressures (Figure 2) and with the *in situ* FTIR spectra (Figures 4 and S6). Again, the term of number of acid site, $[L_A]$, in the left hand side represents the number of acid-base site pairs. It appears that ethanol, and by extension other alcohols, couple via aldol condensation of aldehydes formed by dehydrogenation of the reactant alcohol by direct transfer of H-atoms to the product aldehyde via the MPV reaction. This sequence of steps likely involves kinetically relevant deprotonation of the aldehyde reactants on a surface predominantly covered by ethanol (or ethoxide) species.

These results are consistent with the widely accepted mechanism for the "Guerbet Reaction" of ethanol, which involves aldol condensation for the C–C bond formation reaction between aldehydes,[7,8,22-26,29] but provide new evidence for the pathways for H-transfer, the coverage of reactive species, and the identity of the kinetically relevant step. Scheme 2 summarizes the important reaction boundaries within this system. The kinetic and spectroscopic data suggest that enolate formation is the kinetically relevant step for C–C bond formation in the presence of reactant mixtures containing acetaldehyde and ethanol at 548 K on Ca-HAP. However, this conclusion will not necessarily apply for the rate of formation of 1-butanol or for reactant mixtures containing only ethanol (e.g., ethanol Guerbet reaction), because hydrogen transfer steps that dehydrogenate ethanol and saturate product enals have rates comparable to that for C-C bond formation. The following sections show how these findings can be used to explain, and

predict, the complex product distributions that result from sequences of self- and cross-coupling reactions that occur at longer residence time and at high conversions of ethanol over HAP catalysts.

3.2. Mechanistic Implications of C_n and Branching Distribution of Products

3.2.1. Effects of Reactant Chain Length on Rate Constants for Coupling C_2-C_4 Reactants

1-Butanol and also heavier ($C_{\geq 6}$) products are formed by aldol condensation reactions among $C_{\geq 2}$ aldehydes and subsequent hydrogen transfer by a combination of the MPV and surface mediated H-transfer mechanisms. The $C_{\geq 6}$ products must form by sequential reactions, in which the primary products from aldol condensations of the acetaldehyde condense with other aldehydes ($C_{\geq 2}$) to create secondary products in a cascade of reactions analogous to the primary reaction shown in Scheme 2.[21,22] Consequently, the C_n distribution of the final products reflects the rates at which a given product aldehyde (e.g., C_4H_8O) reacts with any of the other aldehydes present (i.e., C_2–C_{12}).

The rate expression, Eq. (6), can be generalized to describe the C–C bond formation reaction among heavier aldehydes ($C_mH_{2m}O$) with the rate constant for deprotonation (k_5') and the equilibrium constant for desorption (K_4'). The formation of the same C-C bond, between the same reactant aldehydes, can be restated with respect to how it depends on the observed concentration of the reactant alcohol and an apparent rate constant (k_{m-n}) that describes the sequence of adsorption, dehydrogenation, and deprotonation:

$$\frac{r_{C-C}}{[L_A]} = k_5{}'K_4{}'\frac{[C_mH_{2m}O]}{1+K_1[C_2H_5OH]} = k_{m-n}\frac{[C_mH_{2m+1}OH]}{1+K_1[C_2H_5OH]} \qquad (7)$$

where $[C_mH_{2m}O]$ and $[C_mH_{2m+1}OH]$ are gas-phase concentration of C_m aldehydes and alcohols, respectively. While this restated form of the rate equation does not precisely describe the full set of intervening elementary steps, it does provide a conceptual bridge from the fundamental mechanism for C–C bond formation to a functional prediction for the distribution of products formed. The final C_n distribution of the alcohol products depends on the relative values of k_{m-n} for all combinations of *m* (identity of the carbanion) and *n* (the aldehyde which is attacked by the carbanion), which may depend on the size (i.e., C_n) of the reactants.

Figure 5 shows that the rate constants of C–C bond formation, calculated from Eq. 7 for self-coupling (k_{2-2}, k_{3-3}, k_{4-4}) and cross-coupling (k_{2-4}, k_{4-2}) of C_2, C_3, and C_4 aldehydes increase by a factor of two from k_{2-2} to k_{3-3}, after which all value of k_{m-n} are similar among combinations of reactants with C_n greater than two (5 kPa alcohol, 96 kPa H_2, 573 K, 1.67 Ca/P These comparisons (Figure 5) are consistent with previous work that showed empirically fit rate constants for formation of C_4, C_6, and C_8 alcohols to be similar within an order of magnitude during ethanol conversion on Ca-HAP.[21] This indicates that differences between the formation rates of C_4–C_8 species from condensation reactions of C_2–C_4 aldehydes and alcohols depends primarily on the concentration of the reactants and only weakly on the exact identity or structure of the aldehyde intermediates. These findings (Figure 5), together with expectations that further increases in chain length will have a diminished effect on reactivity,[51] suggest that the values of k_{m-n} will be similar for nearly all reactants with three or more C-atoms.

The underlying factors that determine the degree of branching within the products can also be explained by fundamental arguments tied to the mechanism for C–C bond formation. An aldol condensation reaction between two distinct aldehydes (e.g., acetaldehyde and butyraldehyde) forms one of two potential products, and the structure of the product depends on which of the

aldehydes deprotonates prior to nucleophilic attack. Scheme 3 describes the details of the proposed C–C bond formation mechanism between different two aldehyde surface intermediates (possessing alkyl groups R_1 and R_2). Specifically, the deprotonation of aldehyde A with the R_1 group will give a different structural isomers comparing to that of product formed by deprotonation of aldehyde B, containing the R_2 group. Linear products (i.e., n-aldehydes and alcohols) form only when the carbanion forms from acetaldehyde and attacks another normal aldehyde. In contrast, deprotonation of $C_{\geq 4}$ aldehydes ultimately form branched products (i.e., iso-aldehydes and alcohols). Deprotonation energies for aldehydes reflect inductive and resonant effects that depend on the structure of pendant alkyl groups to the carbonyl function,[51] and such changes may influence also the barriers for catalytic reactions that involve deprotonation.

Figure 6 shows that the ratio of formation rates of linear to branched C_6 alcohols ($\gamma = \frac{r_{6,L}}{r_{6,B}}$, where $r_{6,L}$ and $r_{6,B}$ are the formation rates of 1-hexanol and 2-ethyl-butanol, respectively) changes weakly as a function of inverse temperature on Ca-HAP (5 kPa C_2H_5OH, 0.1 kPa C_2H_4O, 0.1 kPa C_4H_8O, 96 kPa H_2, 1.67 Ca/P).[52] When these alcohols are the main products and the amount of other enals or aldehydes are negligible, the ratio of the formation rates of the C_6 products can be restated using the form of the general rate expression (Eq. 7) such that:

$$\gamma = \frac{k_{2-4}[C_2H_4O]}{k_{4-2}[C_4H_8O]} \qquad (8)$$

Thus, γ depends only on the ratio of the rate constants in Eq. 8 when the concentration of C_2 and C_4 aldehydes are equal. Values of γ are near unity (Figure 6) at all temperatures, indicating that the rate constants for these two pathways are similar, which is consistent with comparisons of k_{m-n} values for reactions beginning with alcohols (Figure 5).

The change in the value of γ as a function of temperature reflects the activation enthalpy (ΔH_{C_n}) for each reaction pathway when the rate ratio (Eq. 8) is restated in the form proposed by Eyring:[51]

$$\gamma = A \cdot exp\left(\frac{-(\Delta H_{C_2} - \Delta H_{C_4})}{RT}\right)\frac{[C_2H_4O]}{[C_4H_8O]} \quad (9)$$

where R and T are the universal gas constant and the absolute temperature, ΔH_{C_n} is the apparent activation enthalpy for the pathways that deprotonate each C_n aldehyde species, and A is a pre-factor related to entropic changes, respectively. Therefore, the change in the γ with respect to inverse temperature (Figure 6) reflects the difference between the activation enthalpies for pathways involving deprotonation of acetaldehyde or butyraldehyde ($\Delta\Delta H = \Delta H_{C_2} - \Delta H_{C_4}$). The calculated $\Delta\Delta H$ value (-11 ± 4.9 kJ mol^{-1}) shows that the apparent barrier for acetaldehyde deprotonation is slightly lower than that for butyraldehyde on Ca-HAP, which agrees with the smaller pKa value of acetaldehyde (14.5) than that of butyraldehyde (15.74).[53]

Overall, rate measurements (Figures 5 and 6) show that apparent rate constants for self- and cross-coupling reactions among C_2, C_3, and C_4 species do not vary significantly with C_n of aldehyde or alcohols reactants. Moreover, values of ΔH_{C_n} depend weakly on the structure of the aldehyde that is deprotonated. These trends may be extended to larger C_n species, which would suggest that the specific values of $k_{m\text{-}n}$ (Figure 5) are nearly identical for all alcohols with C_n greater than three. This finding suggests that the final C_n distribution of the products may be predicted without individually measuring rate constants for all possible reaction pathways. In the final section, we show that these product distributions can be predicted for any given extent of conversion using a simple statistical model that exploits the fact that $k_{m\text{-}n}$ values are weakly dependent on the exact structure of the reactant aldehydes and alcohols.

3.3. Cascades of C-C Bond Formation Reaction and Product C_n Distribution

3.3.1. The Factors to Continue the C–C Bond Formation Reaction

Table 2 shows that significant fractions of $C_{\geq 6}$ product alcohols form even at low ethanol conversions on Ca-HAP, and the cascade of coupling reactions responsible for these subsequent steps decreases the yield to 1-butanol. In practice, aldol condensation reactions will continue until all reactive groups for coupling (i.e., –C=O and –COH) are eliminated either by condensation reactions to form larger oxygenates or by dehydration (the major side reaction) of the alcohols to form hydrocarbons. Consequently, the formation of larger alcohol products requires much greater selectivities for alcohol dehydrogenation (Scheme 1, steps 1.2–1.3, and 1.9) and aldol condensation (Scheme 1, steps 1.5–1.8) than those for alcohol dehydration.

The selectivity towards larger alcohols depends on both the reaction temperature and the M/P of the sample. Figure 7a shows that the selectivity to larger alcohols and aldehydes is significantly greater at 573 K than at 623 K at all ethanol conversions over Ca-HAP (5 kPa C_2H_5OH, 96 kPa H_2, 1.67 Ca/P). Specifically, the selectivity towards alcohols and aldehydes is greater than 95% at an ethanol conversion of 55% (Figure 7a). The greater selectivities towards alcohols and aldehydes at 573 K than at 623 K suggest that dehydration has greater apparent activation enthalpies than those for C–C bond formation. Figure 7b shows that the product selectivity depends strongly on the Ca/P ratio of Ca-HAP materials (1.61, 1.67, and 1.74 Ca/P) at all ethanol conversions (5 kPa C_2H_5OH, 96 kPa H_2, 623 K), because the Ca/P ratio largely controls the acid-base character of the surface.[22,23,30] The HAP catalysts with higher base site density, which correlate to higher Ca/P ratio (Table 1), shows higher selectivities to alcohols and aldehydes.

These results, together with Figure S3 and previous discussions, show that lower reaction temperature and use of HAP catalysts with higher densities of base sites and stronger base sites increase selectivities towards C-C bond formation and decrease that for dehydration. Thus, larger ($C_{\geq 6}$) products are obtained at high reactant conversions.

3.3.2. Model Describing the C_n and Branching Distribution of Ethanol Guerbet Products

Figure 8 shows that the selectivity towards larger C_n products (e.g., C_4–C_{12}) increases with ethanol conversion due to secondary self- and cross-condensation reactions among $C_{\geq 2}$ aldehydes over Ca-HAP (5 kPa C_2H_5OH, 96 kPa H_2, 1.67 Ca/P, 573 K) (similar plots for Sr-HAP (1.71 Sr/P) are shown in Figure S7). These larger products include a variety of saturated linear and branched C_4–C_{12} alcohols ($C_{\geq 14}$ alcohols are negligible at these conversion ranges) with a maximum of two ^{3}C-atoms. More than 20 different isomers of C_4–C_{12} alcohols were observed at ethanol conversion of 20% over Ca-HAP, and Figure S8 lists all observed alcohols. The intervening steps that form $C_{\geq 6}$ products are analogous to those shown in Scheme 2, which involves dehydrogenation by the MPV reaction, aldol condensation via kinetically relevant deprotonation of an aldehyde, and sequential MPV and surface mediated hydrogenation steps to form the product alcohols. Below, we show that the resulting distribution of C_n and the mixture of n- and iso-alcohols can be explained by extending the discussions related to the formation of the first C–C bond.

To a first approximation, the condensation reactions within this reaction network can be categorized as either monomer-monomer coupling (i.e., condensation between C_2 aldehydes, also initiation), monomer-oligomer coupling (i.e., condensation between C_2 and $C_{\geq 4}$ aldehydes), or

oligomer-oligomer coupling (i.e., condensation between $C_{\geq 4}$ aldehydes). An average apparent rate constant can be defined to describe each category (i.e., k_{m-m}, k_{m-o}, and k_{o-o}, respectively). Large differences in the values of these rate constants provide different product C_n distributions that evolve in distinct ways as a function of the conversion of the monomer (acetaldehyde) and that of the reactive functional group (i.e., –C=O/–COH). For example, when k_{m-o} is much larger than k_{m-m} or k_{o-o}, the products form by a chain-growth mechanism and the product C_n distribution matches the Anderson-Schulz-Flory model, as seen in Fischer-Tropsch chemistry.[54] Consequently, comparisons of these apparent rate constants can give useful predictions for the products that will form at a given extent of conversion of the reactive species within networks of ethanol-derived species.

For these reaction network, the progress towards completion for condensation reactions is described by the fractional consumption of the initial number of reactive groups (i.e., –C=O derived from –C–OH) and is not well-described by the ethanol conversion. The fraction of reactive groups consumed can be defined as α:[39,40]

$$\alpha = \frac{(N_0 - \sum_{i=2} N_{2i})}{N_0} \qquad (10)$$

where N_0 is the initial number of reactive groups present in the feed (i.e., equal to the number of ethanol molecules) and N_{2i} is the number of reactive groups remaining among all the molecules with carbon number of C_{2i} after a given extent of reaction. Thus, the value of α varies from zero at 0% ethanol conversion to unity when all alcohols and aldehydes, of all C_n, are consumed by condensation or termination (i.e., dehydration) reactions.

Figure 9 shows that the value of α increases on Ca-HAP and Sr-HAP as function of ethanol conversion, controlled by varying the residence time (5 kPa C_2H_5OH, 96 kPa H_2, 573 K). The

precise functional dependence of α on the ethanol conversion reflects the relative rates of monomer–monomer, monomer–oligomer, and oligomer–oligomer condensation reactions, and therefore, also the values of k_{m-m}, k_{m-o}, and k_{o-o}. Figure 9 include curves that show the predicted dependence of α on ethanol conversion for three limiting cases; (1) fast monomer self- and cross-coupling (k_{m-m}, k_{m-o}, >> k_{o-o}), (2) fast oligomer self-coupling (k_{o-o} >> k_{m-m}, k_{m-o}), and (3) equal rate constants for all self- and cross-coupling reactions ($k_{m-m} = k_{m-o} = k_{o-o}$). The experimentally measured relationship between α and ethanol conversion most closely matches the prediction from the third case (i.e., $k_{m-m} = k_{m-o} = k_{o-o}$), commonly known as step-growth polymerization[39,40] and which, for example, describes the polymerization of ε-caprolactam monomers to form Nylon 6. The step growth model predicts the following relationship between α and ethanol conversion (X_{C_2}):[39,40]

$$X_{C_2} = 1 - \frac{N_2}{N_0} = 1 - (1-\alpha)^2 \qquad (11)$$

where N_2 is the number of remaining reactive group of C_2 alcohol in the system (i.e., equal to the number of remaining ethanol molecule). The comparisons between the measured and predicted relationship between α and ethanol conversion (Figure 9), together with the weak dependence of apparent rate constants on the C_n of aldehydes (Figures 5 and 6), show clearly that the network of coupling reaction between ethanol-derived intermediates can be accurately described by a "pseudo step-growth" model (i.e., $k_{m-m} \sim k_{m-o} \sim k_{o-o}$). Thus, the formation rates of products are sensitive only to differences in the gas-phase concentrations of the reactant alcohols and aldehydes.

This generalization model does have one notable exception, because none of the identified alcohols produced in these experiments contain quaternary-carbon atoms (^{4}C-atoms). Based on

the proposed mechanism (Scheme 1) and the accepted mechanism for aldol condensation reactions (Scheme 3), the lack of ^{4}C-containing products shows that alcohols that possess ^{3}C-atom at the α position to the carbonyl have much smaller apparent rate constants for coupling than those for other alcohols. We assume that the unreactive nature of these species is likely caused by steric hindrance which interferes both with deprotonating the ^{3}C-atom and with the nucleophilic attack of the resulting carbanion onto a nearby aldehyde.

Figure 10 shows that the mass fractions of C_4–C_{12} products in the reactor effluent increase nearly monotonically as α increases to a value of 0.3 over Ca-HAP (5 kPa C_2H_5OH, 96 kPa H_2, 573 K, 1.67 Ca/P). The mass fraction of C_n among these C_4–C_{12} products closely match the selectivity for all species predicted by an adapted model for step-growth polymerizations:[39,40]

$$W_{C_{2i}}/W_0 = C_{2i}(1-\alpha)^2\alpha^{(C_{2i}-2)/2} \quad (12)$$

where $W_{C_{2i}}$, W_0, and C_{2i} are the mass of C_{2i} species in the system, the mass of initial monomers, and carbon number of *i*-mers, respectively (dashed lines in Figure 10 portray model predictions). These close comparisons further support the conclusion that a "pseudo step-growth" model and its implicit assumptions provides a functional description of the network of reactions present during the Guerbet reaction of ethanol.[7,8] The product distributions formed over Sr-HAP materials (Figure S9, 5 kPa C_2H_5OH, 96 kPa H_2, 573 K, 1.71 Sr/P) also match the predictions of the ideal step-growth model. These results show also that significant changes to the composition and chemical properties of HAP (i.e., exchange of Sr for Ca) do not influence surface chemistry sufficiently to change the broad nature of the product C_n distributions.

The branching properties of products obtained from Ca- and Sr-HAP catalyst with different M/P ratio are shown in Figure 11. The branching factor for each product is equal to the number of

side-chains (β) and is equal to the number of tertiary C-atoms (^{3}C-atoms) in the molecule (e.g., 1-hexanol and 2-ethyl-1-butanol have β values of 0 and 1, respectively). As mentioned before, no quaternary-carbon atoms (^{4}C-atoms) were observed (Figure S8). Then the averaged branching factor ($\langle\beta\rangle$) for a distribution of products is:

$$\langle\beta\rangle = \frac{\sum P_x \cdot C_{n,x} \cdot \beta_x}{\sum P_x \cdot C_{n,x}} \qquad (13)$$

where P_x, $C_{n,x}$, and β_x are the partial pressure, carbon number, and branching factor of product x, respectively. Figure 11a shows averaged branching factor of the $C_{\geq 4}$ product over Ca-HAP (5 kPa C_2H_5OH, 96 kPa H_2, 573−623 K, 1.67 Ca/P) to show the dependence of reaction temperature. Values of $\langle\beta\rangle$ increase with the progress of the C−C bond formation reaction due to the continuous and irreversible formation of branched products.$\langle\beta\rangle$ values decrease slightly with increasing temperature (Figure 11a), however, this change is solely a consequence of the more significant rates of dehydration (i.e., termination, Figure 7a), which increase α values but do not form new C-C bonds, increase the C_n of the products, or introduce new ^{3}C-atoms into the product distribution. Values of $\langle\beta\rangle$ values change slightly with the M/P ratio (Figure 11b), although these changes are primarily the result of greater termination rates that produce linear C_4 hydrocarbons (Figure 7b). Ca-HAP material (1.67 Ca/P) produces slightly more linear products than do Sr-HAP (1.71 Sr/P) (Figure 11c), which likely reflects the higher base site density (Table 1) of Sr-containing HAP, although the difference is not so significant. Overall, the small changes in $\langle\beta\rangle$ values attributable to differences in self- and cross-coupling aldol condensation rates (Figure 11) suggest that we have a little room to control the product C_n and branching distribution properties by simple changes to the composition and active site identities of HAP catalysts. Together the broad C_n distributions (Figures 9, 10, and S9) and the lack of control over product branching

(Figure 11) observed for all HAP catalysts studied (Ca- or Sr-HAP with $1.61 \leq M/P \leq 1.74$) suggest that the structure of the product alcohols that form do not depend in any significant manner on the surface composition or chemical properties of HAP catalysts. Thus, it appears that ethanol coupling reactions over HAP cannot provide narrow distributions of aliphatic alcohols or reasonable selectivities to any given alcohol (e.g., 1-butanol or 1-octanol). Thus, reaction networks involving aldol condensations need to involve reaction intermediates with vastly different tendencies towards enolization or to form products that are effectively self-terminated in order to create narrow product distributions.

Conclusions

In the present study, the detailed mechanism of C−C bond formation of ethanol coupling and the distribution of products following the continuous condensation reactions were investigated over hydroxyapatite (HAP) catalysts using a combination of rate measurements, *in situ* FTIR spectroscopy, isotope labelling experiments, and comparisons of product distributions to simple models. C−C bond formation occurs by a sequence of steps, which hydrogen transfer and aldol condensation of two aldehyde intermediates. Rates of C–C bond formation depend linearly on acetaldehyde pressure and possess a negative dependence on ethanol pressure ($r_{C-C} \sim [C_2H_5OH]^{-0.3\pm0.2}$). Kinetic measurements and *in situ* spectroscopy show that ethanol derived surface species are among the most abundant reactive intermediates and the coverage of acetaldehyde is much smaller. Together these data and their interpretation clarify the reaction network that forms C–C bonds among reactant mixtures containing both acetaldehyde and ethanol at 548 K on Ca-HAP. At these conditions, C–C bonds form via a kinetically relevant deprotonation step of the α-carbon of aldehydes on ethanol-covered HAP surfaces. Isotope labeling experiments show that the Meerwein-Ponndorf-Verley reaction produces reactive aldehyde intermediates and hydrogenates C=O bonds of aldol products (e.g., crotonaldehyde) by a direct intermolecular hydrogen transfer pathway. However, C=C bonds hydrogenate via surface mediated H-transfer pathways, which have lower rate constant than those for the MPV reaction. Thus, product distributions show high selectivities towards enols as compared to aldehydes at these conditions. Rate measurements of self- and cross-coupling reactions among C_2−C_4 species vary within a factor of two, and apparent activation enthalpy values depend weakly on the carbon number of the aldehyde that is deprotonated. Comparisons between ethanol conversion and the fractional conversion of all reactive groups (α: describing the progress of the

continuous reaction) show that an adapted step-growth polymerization model accurately predicts the distribution of carbon numbers among the products of this reaction network, which is consistent also with the assumption that pseudo-first order rate constants for all coupling reactions are nearly similar. These results, however, suggest there is little that can be done to control the product distribution and branching properties even by modifying reaction temperature and base site densities. These findings will introduce the idea that design of a catalyst that can change apparent rate for different C_{2i} species allow fine tuning of product distribution.

Acknowledgements

The authors gratefully acknowledge Mr. Andrew Rowley for his help synthesizing catalysts and collecting and analyzing experimental data. This work was financially supported by the Energy Biosciences Institute (EBI) at the University of Illinois. This work was carried out in part in the Frederick Seitz Materials Research Laboratory, University of Illinois.

References

(1) Climent, M. J.; Corma, A.; Iborra, S. *Green Chem.* **2014**, *16*, 516–547.

(2) World Energy Outlook 2014; **2014**. http://www.worldenergyoutlook.org/publications/weo-2014/. (accessed Apr 6, 2016)

(3) Serrano-Ruiz, J. C.; Dumesic, J. A. *Energy Environ. Sci.* **2011**, *4*, 83–99.

(4) Demirbas, A. *Prog. Energy Combust. Sci.* **2007**, *33*, 1–18.

(5) Balat, M.; Balat, H.; Oz, C. *Prog. Energy Combust. Sci.* **2008**, *34*, 551–573.

(6) IEA Energy Technology Essentials: Biofuel Production; **2007**. https://www.iea.org/publications/freepublications/publication/essentials2.pdf. (accessed Apr 6, 2016)

(7) Kozlowski, J. T.; Davis, R. J. *ACS Catal.* **2013**, *3*, 1588–1600.

(8) Gabriëls, D.; Hernández, W. Y.; Sels, B.; Voort, P. V. D.; Verberckmoes, A. *Catal Sci Technol.* **2015**, *5*, 3876–3902.

(9) Anbarasan, P.; Baer, Z. C.; Sreekumar, S.; Gross, E.; Binder, J. B.; Blanch, H. W.; Clark, D. S.; Toste, F. D. *Nature* **2012**, *491*, 235–239.

(10) Sun, J.; Wang, Y. *ACS Catal*. **2014**, *4*, 1078–1090.

(11) Angelici, C.; Weckhuysen, B. M.; Bruijnincx, P. C. A. *ChemSusChem* **2013**, *6*, 1595–1614.

(12) Ueda, W.; Kuwabara, T.; Ohshida, T.; Morikawa, Y. *J. Chem. Soc., Chem. Comm.* **1990**, 1558–1559.

(13) Ueda, W.; Ohshida, T.; Kuwabara, T.; Morikawa, Y. *Catal. Lett.* **1992**, *12*, 97–104.

(14) Chieregato, A.; Velasquez Ochoa, J.; Bandinelli, C.; Fornasari, G.; Cavani, F.; Mella, M. *ChemSusChem* **2015**, *8*, 377–388.

(15) Ndou, A. *Appl. Catal., A* **2003**, *251*, 337–345.

(16) Marcu, I.-C.; Tanchoux, N.; Fajula, F.; Tichit, D. *Catal. Lett.* **2012**, *143*, 23–30.

(17) Carvalho, D. L.; de Avillez, R. R.; Rodrigues, M. T.; Borges, L. E. P.; Appel, L. G. *Appl. Catal., A* **2012**, *415–416*, 96–100.

(18) Ordóñez, S.; Díaz, E.; León, M.; Faba, L. *Catal. Today* **2011**, *167*, 71–76.

(19) Di Cosimo, J. I.; Apesteguía, C. R.; Ginés, M. J. L.; Iglesia, E. *J. Catal.* **2000**, *190*, 261–275.

(20) Gines, M. J. L.; Iglesia, E. *J. Catal.* **1998**, *176*, 155–172.

(21) Tsuchida, T.; Sakuma, S.; Takeguchi, T.; Ueda, W. *Ind. Engi. Chem. Res.* **2006**, *45*, 8634–8642.

(22) Tsuchida, T.; Kubo, J.; Yoshioka, T.; Sakuma, S.; Takeguchi, T.; Ueda, W. *J. Catal.* **2008**, *259*, 183–189.

(23) Ogo, S.; Onda, A.; Iwasa, Y.; Hara, K.; Fukuoka, A.; Yanagisawa, K. *J. Catal.* **2012**, *296*, 24–30.

(24) Ogo, S.; Onda, A.; Yanagisawa, K. *Appl. Catal., A* **2011**, *402*, 188–195.

(25) Silvester, L.; Lamonier, J.-F.; Faye, J.; Capron, M.; Vannier, R.-N.; Lamonier, C.; Dubois, J.-L.; Couturier, J.-L.; Calais, C.; Dumeignil, F. *Catal. Sci. Technol.* **2015**, *5*, 2994–3006.

(26) Ho, C. R.; Shylesh, S.; Bell, A. T. *ACS Catal.* **2015**, *6*, 939-948.

(27) Scalbert, J.; Thibault-Starzyk, F.; Jacquot, R.; Morvan, D.; Meunier, F. *J. Catal.* **2014**, *311*, 28–32.

(28) C. Meunier, F.; Scalbert, J.; Thibault-Starzyk, F. *C. R. Chim.* **2015**, *18*, 345–350.

(29) Hanspal, S.; Young, Z. D.; Shou, H.; Davis, R. J. *ACS Catal.* **2015**, *5*, 1737–1746.

(30) Tsuchida, T.; Kubo, J.; Yoshioka, T.; Sakuma, S.; Takeguchi, T.; Ueda, W. *J. Jpn. Pet. Inst.* **2009**, *52*, 51–59.

(31) Black, G.; Curran, H. J.; Pichon, S.; Simmie, J. M.; Zhukov, V. *Combust. Flame* **2010**, *157*, 363–373.

(32) Rakopoulos, D. C.; Rakopoulos, C. D.; Hountalas, D. T.; Kakaras, E. C.; Giakoumis, E. G.; Papagiannakis, R. G. *Fuel* **2010**, *89*, 2781–2790.

(33) Alonso, D. M.; Bond, J. Q.; Dumesic, J. A. *Green Chem.* **2010**, *12*, 1493–1513.

(34) Nagaraja.V *Indian J. Technol.* **1971**, *9*, 380–386.

(35) Diallo-Garcia, S.; Laurencin, D.; Krafft, J.-M.; Casale, S.; Smith, M. E.; Lauron-Pernot, H.; Costentin, G. *J. Phys. Chem. C* **2011**, *115*, 24317–24327.

(36) Diallo-Garcia, S.; Osman, M. B.; Krafft, J.-M.; Casale, S.; Thomas, C.; Kubo, J.; Costentin, G. *J. Phys. Chem. C* **2014**, *118*, 12744–12757.

(37) Hill, I. M.; Hanspal, S.; Young, Z. D.; Davis, R. J. *J. Phys. Chem. C* **2015**, *119*, 9186–9197.

(38) Witzke, M. E.; Dietrich, P.; Ibrahim, M.; Al-Bardan, K.; Triezenberg, M.; Flaherty, D. W. to be submitted.

(39) Stille, J. K. *J. Chem. Educ.* **1981**, *58*, 862–866.

(40) Fried, J. R. *Polymer Science and Technology,* 3rd ed.; Prentice Hall; 2014.

(41) Wang, J.; Kispersky, V. F.; Nicholas Delgass, W.; Ribeiro, F. H. *J. Catal.* **2012**, *289*, 171–178.

(42) r_{C-C} is not equal to the butanol formation rate or ethanol conversion rate, which does not include contributions from C_4 species that are not fully hydrogenated (i.e., crotonaldehyde, crotyl alcohol, and butyraldehyde)

(43) Gilkey, M. J.; Xu, B. *ACS Catal.* **2016**, *6*, 1420–1436.

(44) Kibby, C. L.; Hall, W. K. *J. Catal.* **1973**, *31*, 65–73.

(45) Gilkey, M. J.; Panagiotopoulou, P.; Mironenko, A. V.; Jenness, G. R.; Vlachos, D. G.; Xu, B. *ACS Catal*. **2015**, *5*, 3988–3994.

(46) Suzuoki, T.; Epstein, S. *Geochim. Cosmochim. Acta.* **1976**, *40*, 1229–1240.

(47) Stošić, D.; Bennici, S.; Sirotin, S.; Calais, C.; Couturier, J.-L.; Dubois, J.-L.; Travert, A.; Auroux, A. *Appl. Catal., A* **2012**, *447–448*, 124–134.

(48) Ramesh, K.; Ling, E. G. Y.; Gwie, C. G.; White, T. J.; Borgna, A. *J. Phys. Chem. C* **2012**, *116*, 18736–18745.

(49) Faria, R. M. B.; Cesar, D. V.; Salim, V. M. M. *Catal. Today* **2008**, *133*, 168–173.

(50) Griffiths, P. R.; Haseth, J. A. D. *Fourier Transform Infrared Spectrometry*, 2nd ed.; John Wiley & Sons, Inc.: Hoboken, New Jersey, 2007.

(51) Anslyn, E. V.; Dougherty, D. A. *Modern Physical Organic Chemistry*; University Science Books: Sausalito, California, 2005.

(52) The secondary products formed from C_6 alcohols are accounted in these primary products.

(53) ChemAxon, **2016**. https://www.ChemAxon.com. (accessed Apr 6, 2016)

(54) Biloen, P.; Sachtler, W. M. H. *In Advances in Catalysis*; D. D. Eley, H. P.; Paul, B. W., Eds.; Academic Press: New York, 1981; Vol. *30*, pp 165–216.

Table 1. Properties of Ca- and Sr-HAP catalysts.

Sample #	Product Phase[a]	M/P ratio[b]	Specific surface area[c] (m^2 g^{-1})	Specific surface area[c] (m^2 $mmol^{-1}$)	Base site density[d] (μmol m^{-2})	Stronger basic site density[d] (μmol m^{-2})
1	Ca-HAP	1.61	70	35	0.74	0.09
2	Ca-HAP	1.67	66	33	1.4	0.54
3	Ca-HAP	1.74	66	33	2.6	0.87
4	Sr-HAP	1.62	38	28	0.56	0.20
5	Sr-HAP	1.71	37	27	1.5	0.48

a: Confirmed by XRD, b: Measured by ICP, c: Measured by N_2 adsorption, d: Measured by CO_2-TPD, Total and stronger base site densities are calculated by measuring the adsorbed amounts of CO_2 between 300–500 K and 400–500 K, respectively.

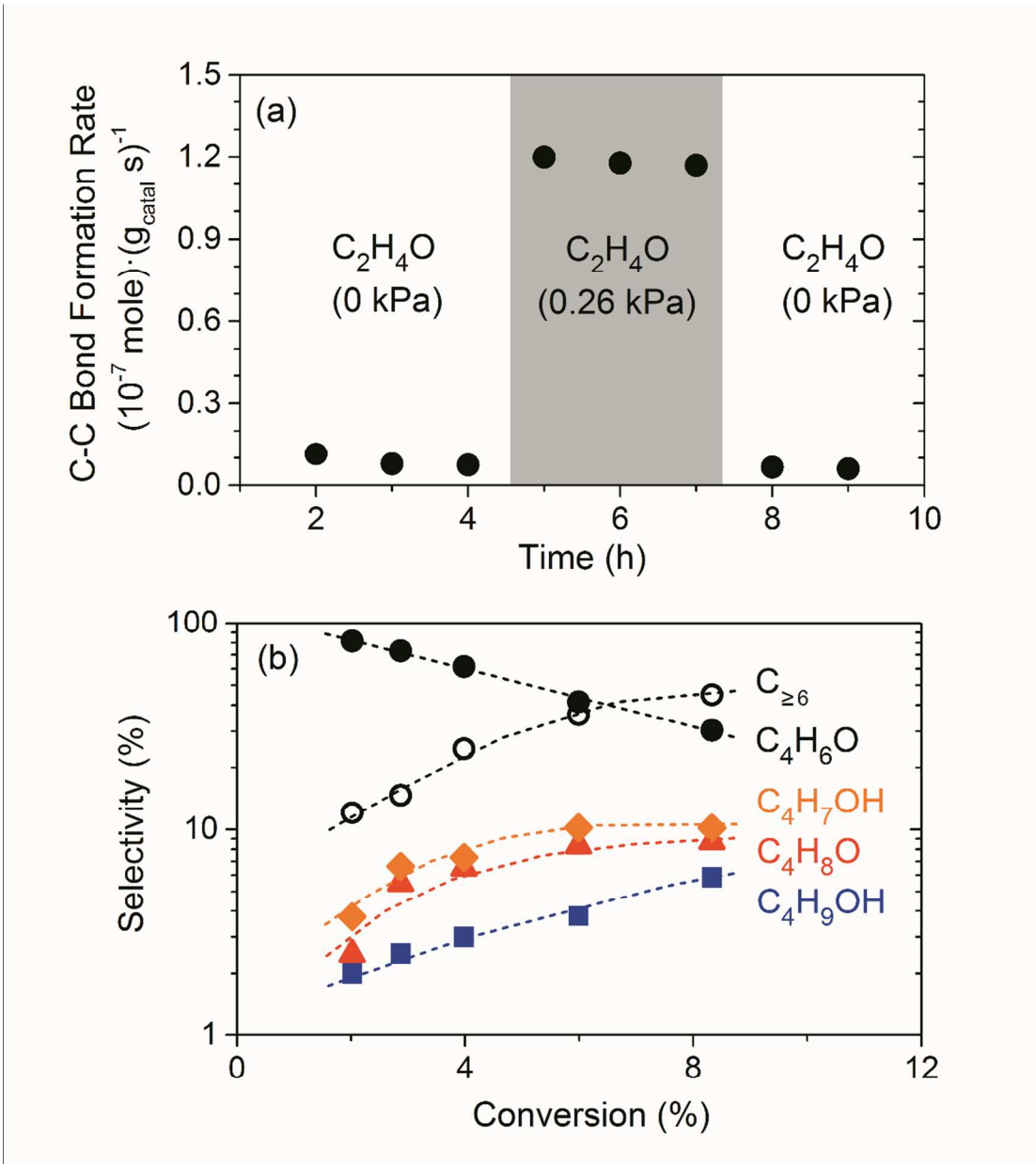

Figure 1. Effect of co-feeding acetaldehyde. (a) Changes in the C–C bond formation rates with or without 0.26 kPa C_2H_4O on Ca-HAP (4.8 kPa C_2H_5OH, 96 kPa H_2, 1.67 Ca/P, 548 K). (b) Change in the product selectivities towards crotonaldehyde (black ○), butyraldehyde (red ▲), crotyl alcohol (orange ♦), butanol (blue ■), and $C_{\geq 6}$ products (black ●) on Ca-HAP with low ethanol pressure (1 kPa C_2H_5OH, 0.35 kPa C_2H_4O, 100 kPa H_2, 1.67 Ca/P, 548 K). Dashed lines in the figures are meant to guide the eye.

Table 2. Product selectivities at 3% and 8% conversion of C_2 reactant pool on Ca-HAP (1.0–4.8 kPa C_2H_5OH, 0–0.35 kPa C_2H_4O, Balance H_2, 1.67 Ca/P, 548 K).

Ethanol pressure (kPa)	4.8	4.8	4.8	1.0
Acetaldehyde pressure (kPa)	0	0	0.26	0.35
C_2 reactant conversion[a] (%)	3.3	8.2	8.1	8.3
Ethylene	4.6	3.5	3.6	tr.
Ethane	tr.	0.8	tr.	tr.
Butyraldehyde	tr.	tr.	1.8	8.7
Crotonaldehyde	tr.	tr.	2.2	30.4
1-butanol	79.2	81.7	62.0	5.9
Crotyl alcohol	11.4	4.3	14.5	10.2
C_6 alcohols and aldehydes	4.4	7.6	10.1	15.1
C_8 alcohols and aldehydes	0.1	0.6	0.4	1.7
Aromatics	tr.	tr.	tr.	26.0
Others	0.2	1.5	5.4	2.0

[a]: C_2 reactant is ethanol and acetaldehyde.

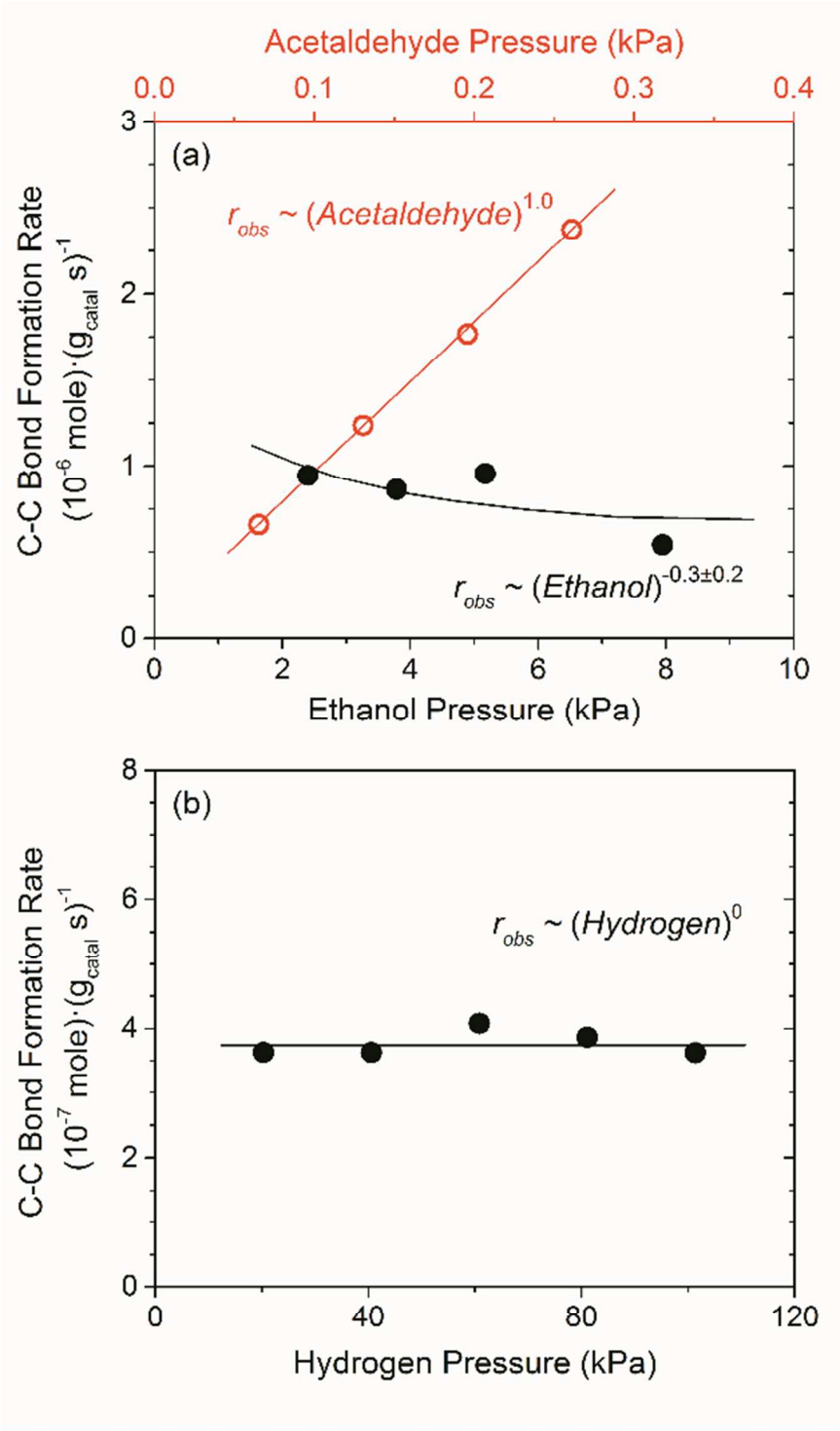

Figure 2. Change in the C–C bond formation rate on Ca-HAP (1.67 Ca/P) at 548 K as function of (a) acetaldehyde pressure (4.8 kPa C_2H_5OH, 96 kPa H_2) and ethanol pressure (0.1 kPa C_2H_4O, 96 kPa H_2), and (b) hydrogen pressure (5 kPa C_2H_5OH, balance He).

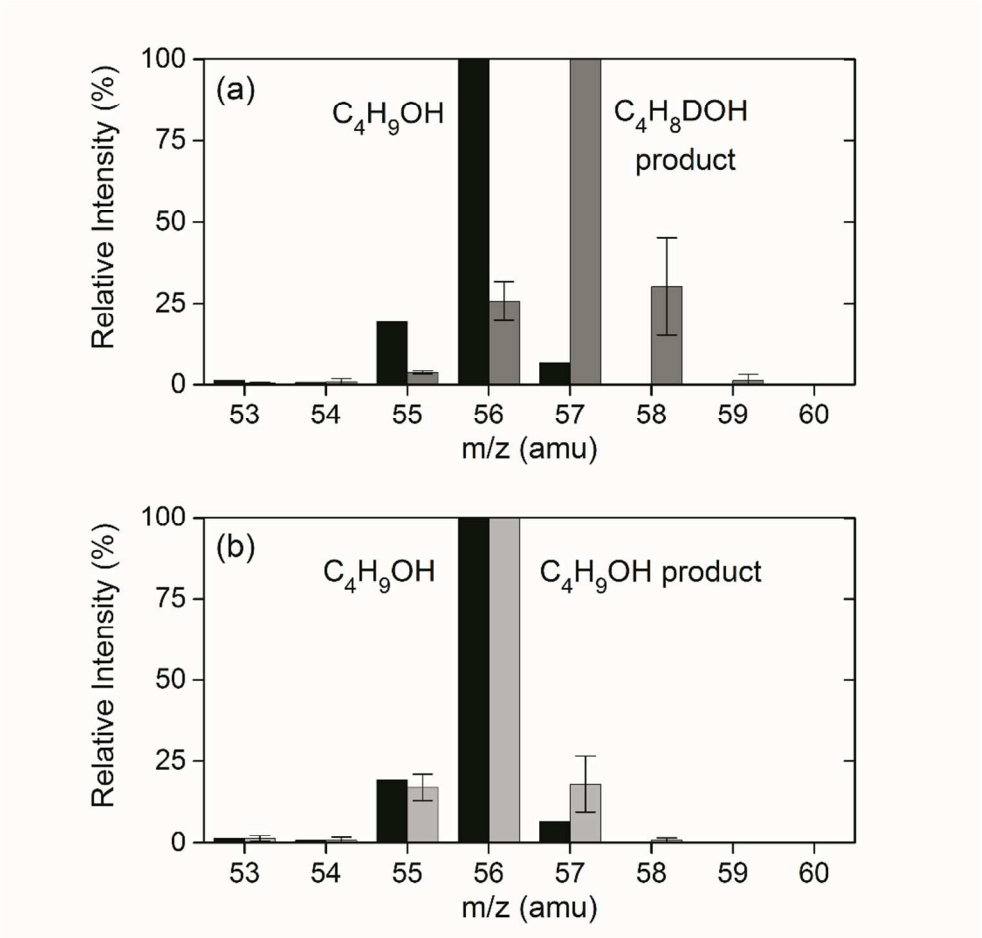

Figure 3. Mass spectrum of 1-butanol obtained from the hydrogenation of (a) butyraldehyde (dark grey) or (b) crotyl alcohol (light grey) with labeled 2-propanol under excess amount of *tert*-butanol on Ca-HAP (0.5 kPa C_4H_8O or C_4H_7OH, 0.6 kPa C_3D_7OD, 2.4 kPa *tert*-C_4H_9OH, 97 kPa H_2, 1.67 Ca/P, 573 K), and those products containing purely hydrogen (black; as a reference).

$$C_2H_5OH + *_A \rightleftarrows C_2H_5OH*_A \quad (1.1)$$
$$C_2H_5OH*_A + *_B \rightleftarrows C_2H_5O*_A + H*_B \quad (1.2)$$
$$C_2H_5O*_A + *_B \rightleftarrows C_2H_4O*_A + H*_B \quad (1.3)$$
$$C_2H_4O + *_A \rightleftarrows C_2H_4O*_A \quad (1.4)$$
$$C_2H_4O*_A + *_B \rightarrow C_2H_3O*_A + H*_B \quad (1.5)$$
$$C_2H_3O*_A + C_2H_4O*_A \rightleftarrows C_4H_7O_2*_A + *_A \quad (1.6)$$
$$C_4H_7O_2*_A + H*_B \rightleftarrows C_4H_8O_2*_A + *_B \quad (1.7)$$
$$C_4H_8O_2*_A + *_A \rightleftarrows C_4H_6O*_A + H_2O*_A \quad (1.8)$$
$$C_4H_6O*_A + C_2H_5OH*_A \rightleftarrows C_4H_7OH*_A + C_2H_4O*_A \quad (1.9)$$
$$C_4H_7OH*_A + 2H*_B \rightleftarrows C_4H_9OH*_A + 2*_B \quad (1.10)$$
$$C_4H_6O*_A \rightleftarrows C_4H_6O + *_A \quad (1.11)$$
$$C_4H_7OH*_A \rightleftarrows C_4H_7OH + *_A \quad (1.12)$$
$$C_4H_9OH*_A \rightleftarrows C_4H_9OH + *_A \quad (1.13)$$
$$2H*_B \rightleftarrows H_2 + 2*_B \quad (1.14)$$

Scheme 1. Proposed sequence of steps for C–C reactions among ethanol and ethanol-derived species on HAP catalysts. $*_A$ and $*_B$ denote unoccupied surface acid and base sites, respectively; *X* and *X** represents a gas-phase and bound surface intermediate, respectively; ⇄ indicates that the elementary step is quasi-equilibrated; → indicates that the elementary step is kinetically relevant and irreversible.

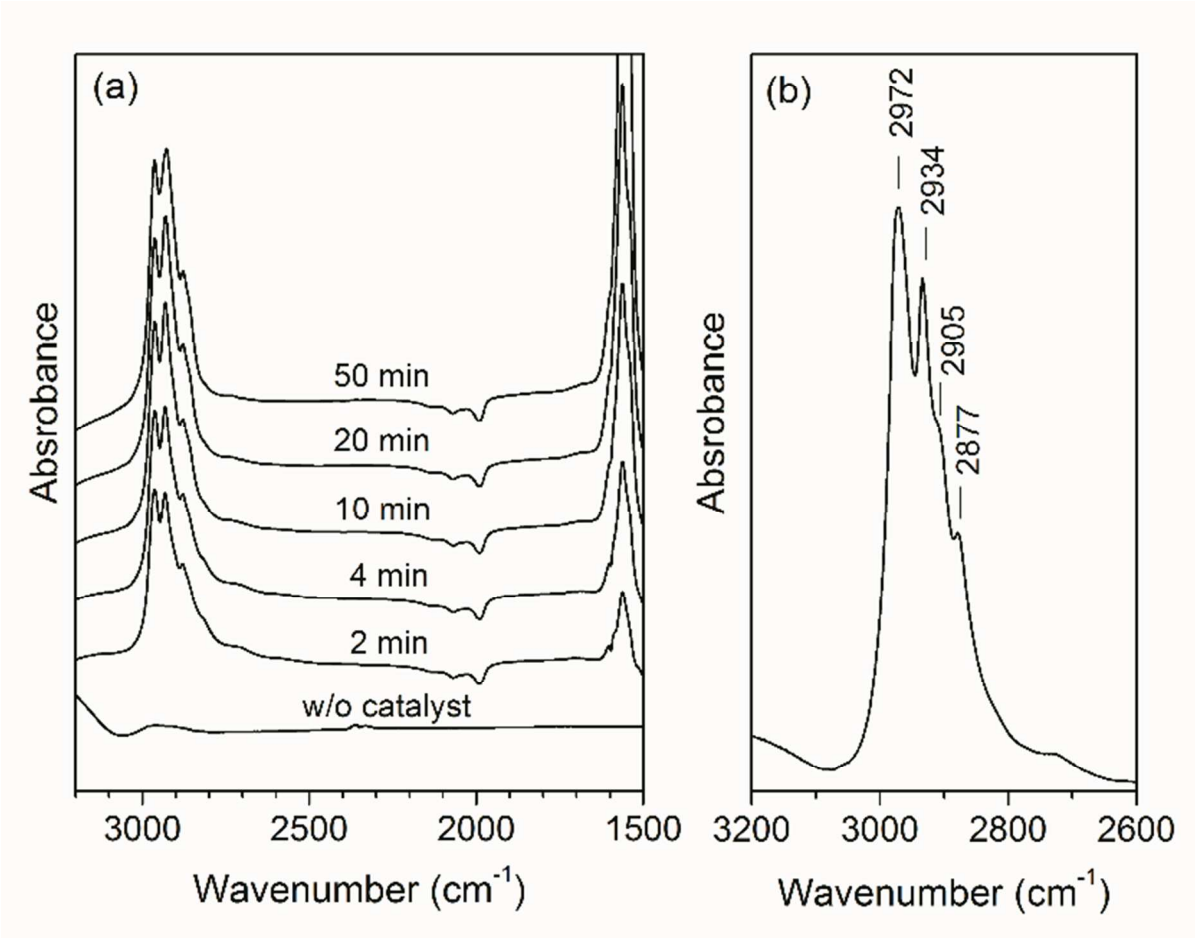

Figure 4. *In situ* FTIR spectra of surface species that form on the Ca-HAP catalyst at standard ethanol coupling conditions (4.6 kPa C_2H_5OH, 96 kPa H_2, 573 K, 1.67 Ca/P). (a) Spectrum measured without catalyst (bottom, control measurement) and spectra measured after the feeding of ethanol for 2, 4, 10, 20, and 50 min (bottom to top). (b) Spectrum of the reactive surface species obtained by subtracting the FTIR spectrum of the persistent aromatic surface species.

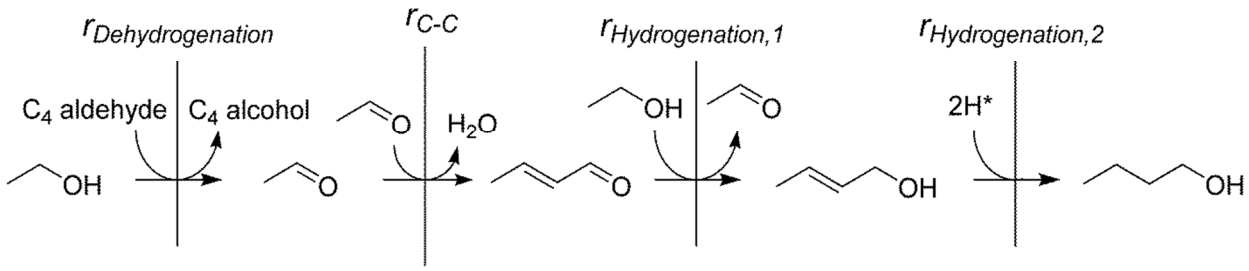

Scheme 2. Demarcation of important boundaries, observed intermediates, and the associated rates involved in the formation of n-butanol from ethanol and ethanol-derived reactants. The sequence of reactions includes dehydrogenation of alcohols ($r_{Dehydrogenation}$), C–C bond formation by condensation reactions of aldehydes ($r_{C–C}$), and subsequent two types of hydrogenation steps to form enols ($r_{Hydrogenation,1}$) and then butanol ($r_{Hydrogenation,2}$).

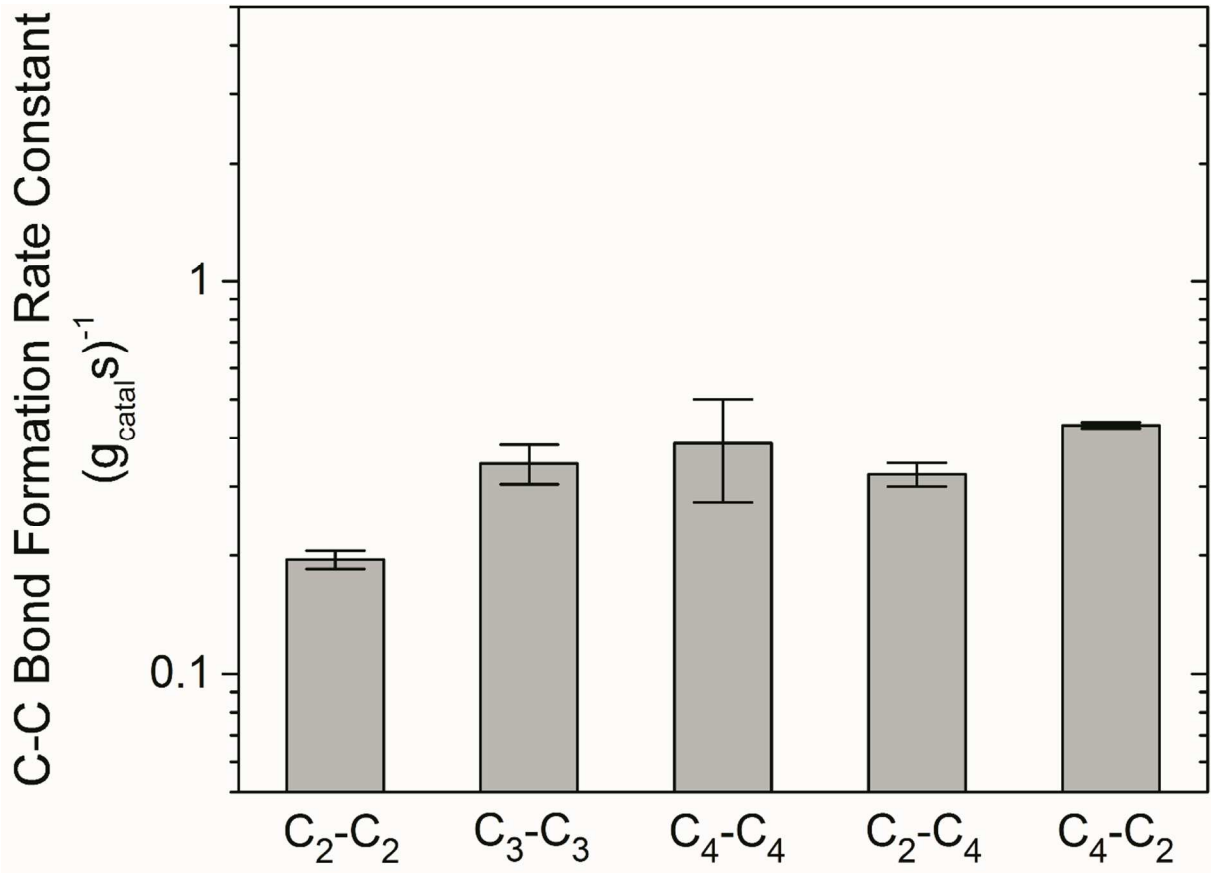

Figure 5. The changes of rate constants for self- and cross-coupling reaction among C_2, C_3, and C_4 alcohols over Ca-HAP (5 kPa alcohols, 96 kPa H_2, 1.67 Ca/P, 573 K).

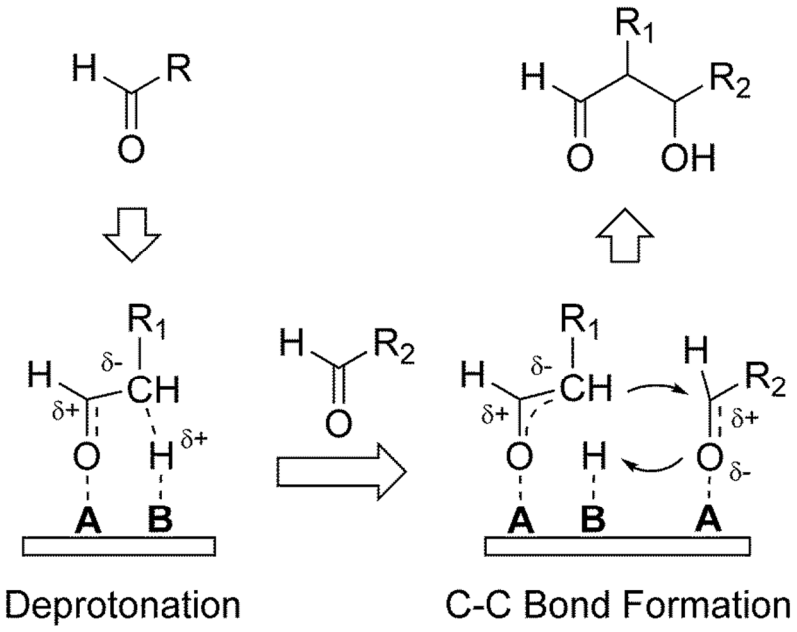

Scheme 3. Schematic depiction of aldol condensation on a HAP surface. **A** and **B** in the scheme denotes acid and base sites, respectively. A base site deprotonates the α-carbon of an aldehyde adsorbed to a vicinal acid site to form an enolate, which can nucleophilically attack an adjacent adsorbed aldehyde to form a C–C bond between the α- and β-carbon of the aldehyde and enolate, respectively. The isomeric structure of the resulting aldol, and the subsequent enal, aldehyde, and alcohol products, depends on the individual identities of the R_1 and R_2.

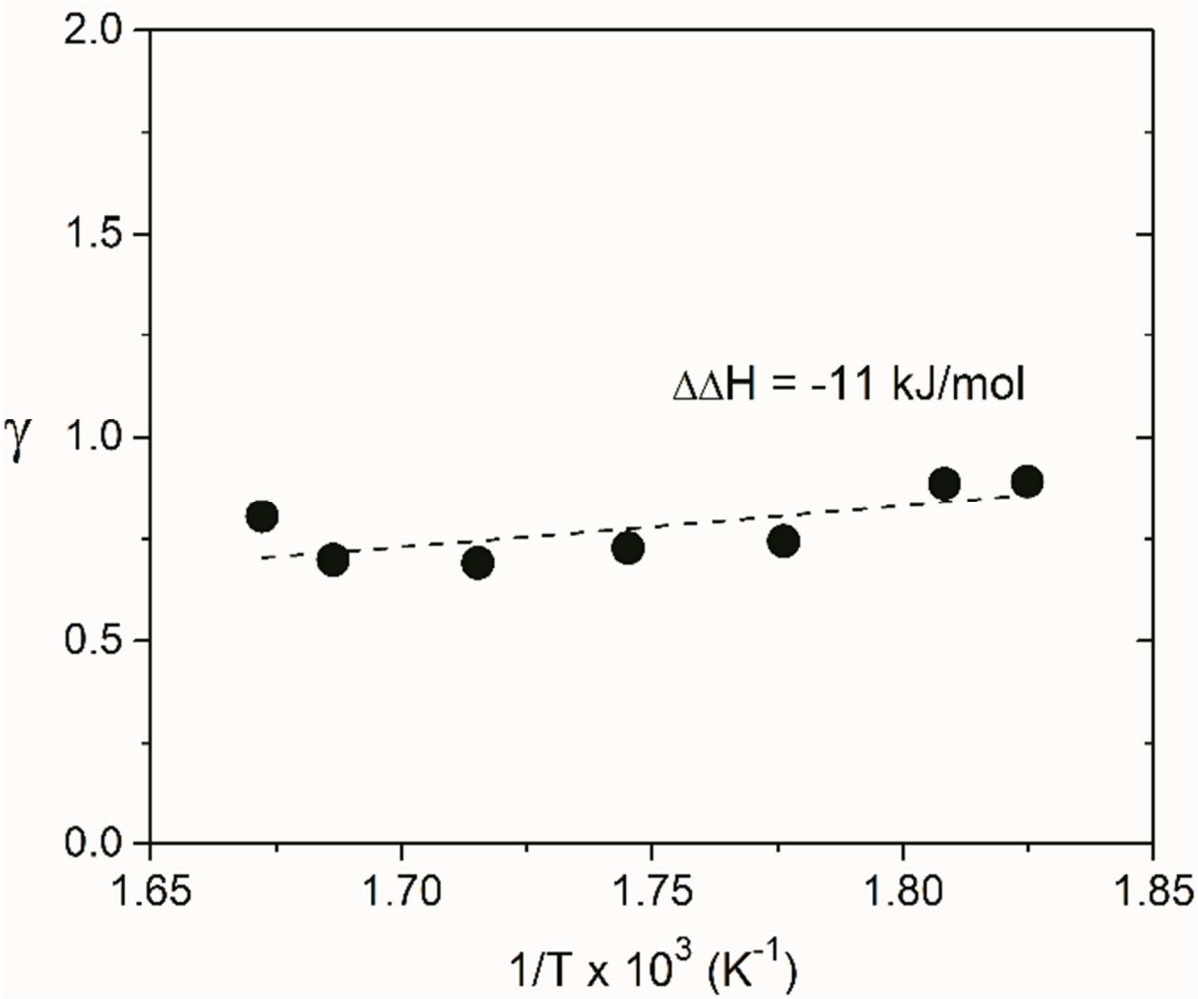

Figure 6. The ratio of the concentration of linear to branched C_6 alcohols (i.e., 1-hexanol and 2-ethyl-butanol, respectively), γ, produced by coupling reactions among acetaldehyde and butyraldehyde reactants over Ca-HAP as a function of inverse temperature (0.1 kPa C_2H_4O, 0.1 kPa C_4H_8O, 5 kPa C_2H_5OH, 96 kPa H_2, 1.67 Ca/P, 548–598 K). Dashed line in the figure represents the exponential fit to the data.

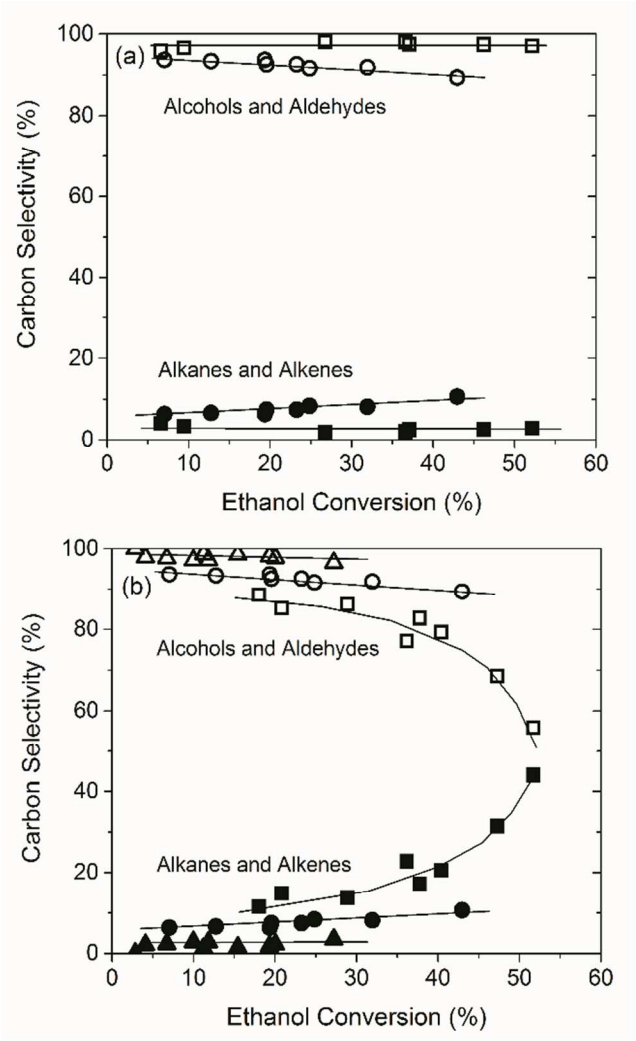

Figure 7. The change in the product selectivity during coupling reactions of ethanol-derived intermediates as functions of ethanol conversion, controlled by varying the residence time, on Ca-HAP materials (5 kPa C_2H_5OH, 96 kPa H_2). (a) Changes in selectivities towardsalcohols-aldehydes(○, 573 K; □, 623 K) and alkenes-alkanes (●, 573 K; ■, 623 K) from a change in the reaction temperature on Ca-HAP (1.67 Ca/P). (b) Dependence of the product selectivities (alcohols-aldehydes (solid symbols); alkanes-alkenes (open symbols)) on the Ca/P ratios within a series of Ca-HAP materials with Ca/P ratios of 1.61 (■, □), 1.67 (●, ○), and 1.74 (▲, △) at 623 K. Solid lines in the figures are meant to guide the eye.

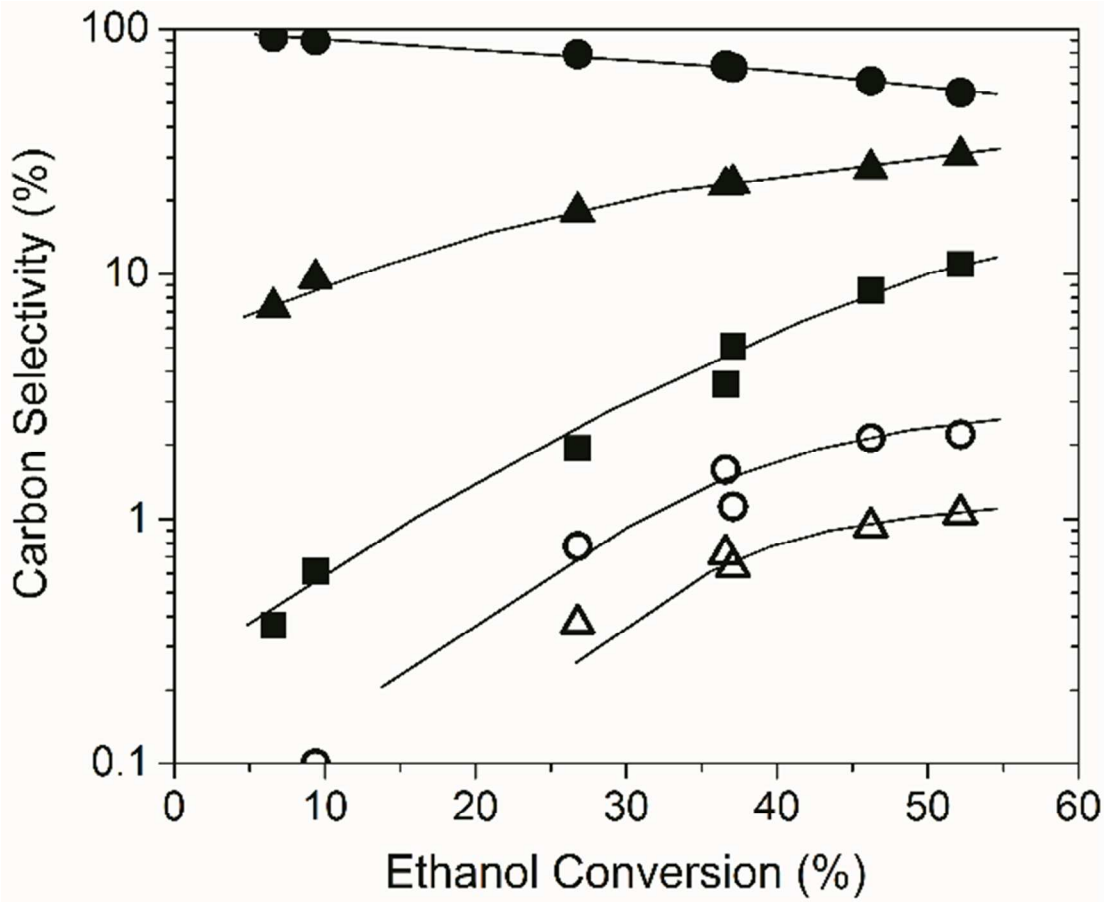

Figure 8. The change in the carbon product selectivity to C_4 (●), C_6 (▲), C_8 (■), C_{10} (○), and C_{12} (△) alcohols and aldehydes during condensation reactions of ethanol-derived intermediates as function of ethanol conversion, controlled by varying the residence time on Ca-HAP (5 kPa C_2H_5OH, 96 kPa H_2, 1.67 Ca/P, 573 K). Solid lines in the figures are included to guide the eye.

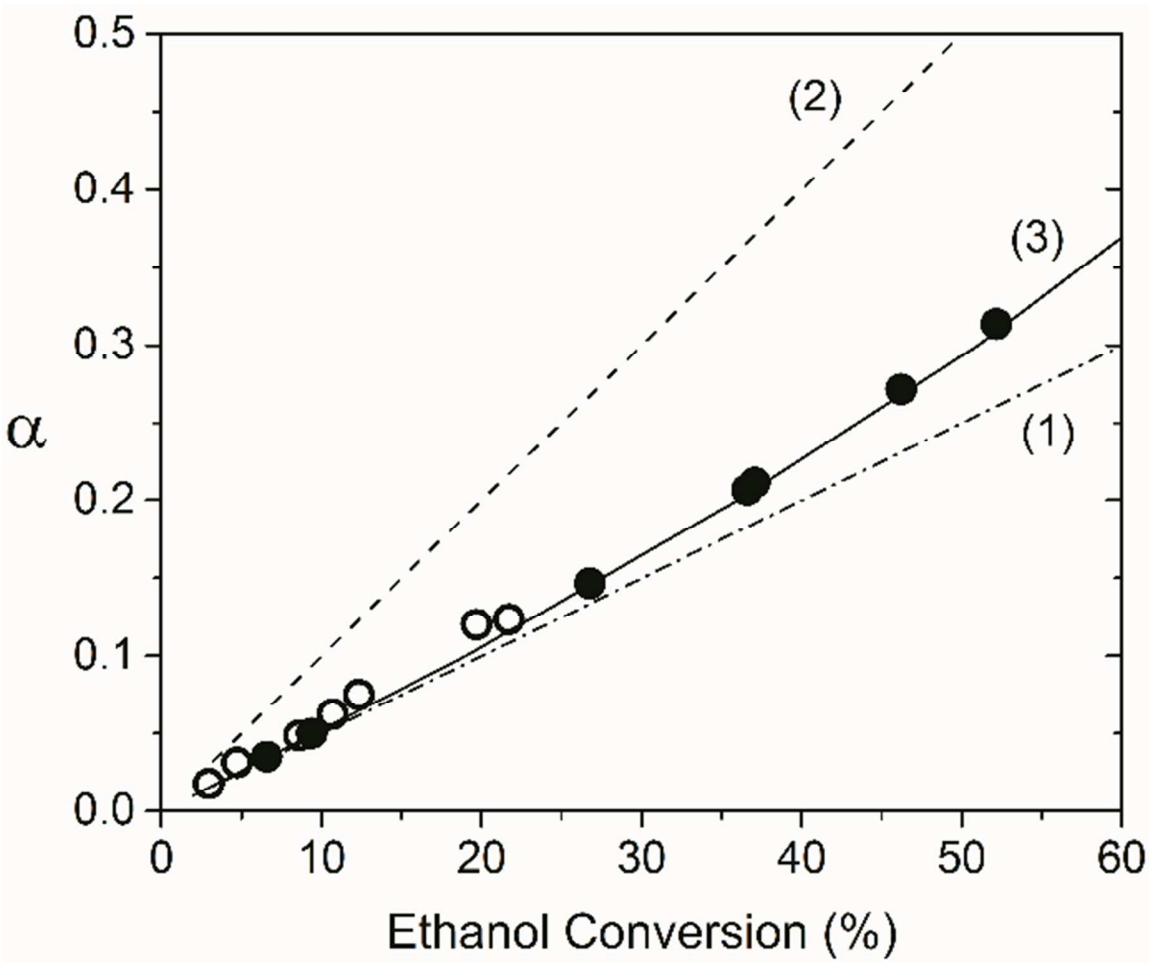

Figure 9. Measured value of α on Ca-HAP catalyst with Ca/P ratio of 1.67 (●) and Sr-HAP catalyst with Sr/P ratio of 1.71 (○) (5 kPa C_2H_5OH, 96 kPa H_2, 573 K) as function of ethanol conversion, controlled by varying the residence time. Three lines represent three assumed models; (1) monomers condense more easily than reactions between oligomers (fast monomer coupling, k_{m-m}, k_{m-o}, >> k_{o-o}, – · –), (2) reactions of oligomers are more facile than any reactions involving monomers (fast oligomer self-coupling, k_{o-o} >> k_{m-m}, k_{m-o}, ----), and (3) all condensation steps have similar rate constants ($k_{m-m} = k_{m-o} = k_{o-o}$, ——).

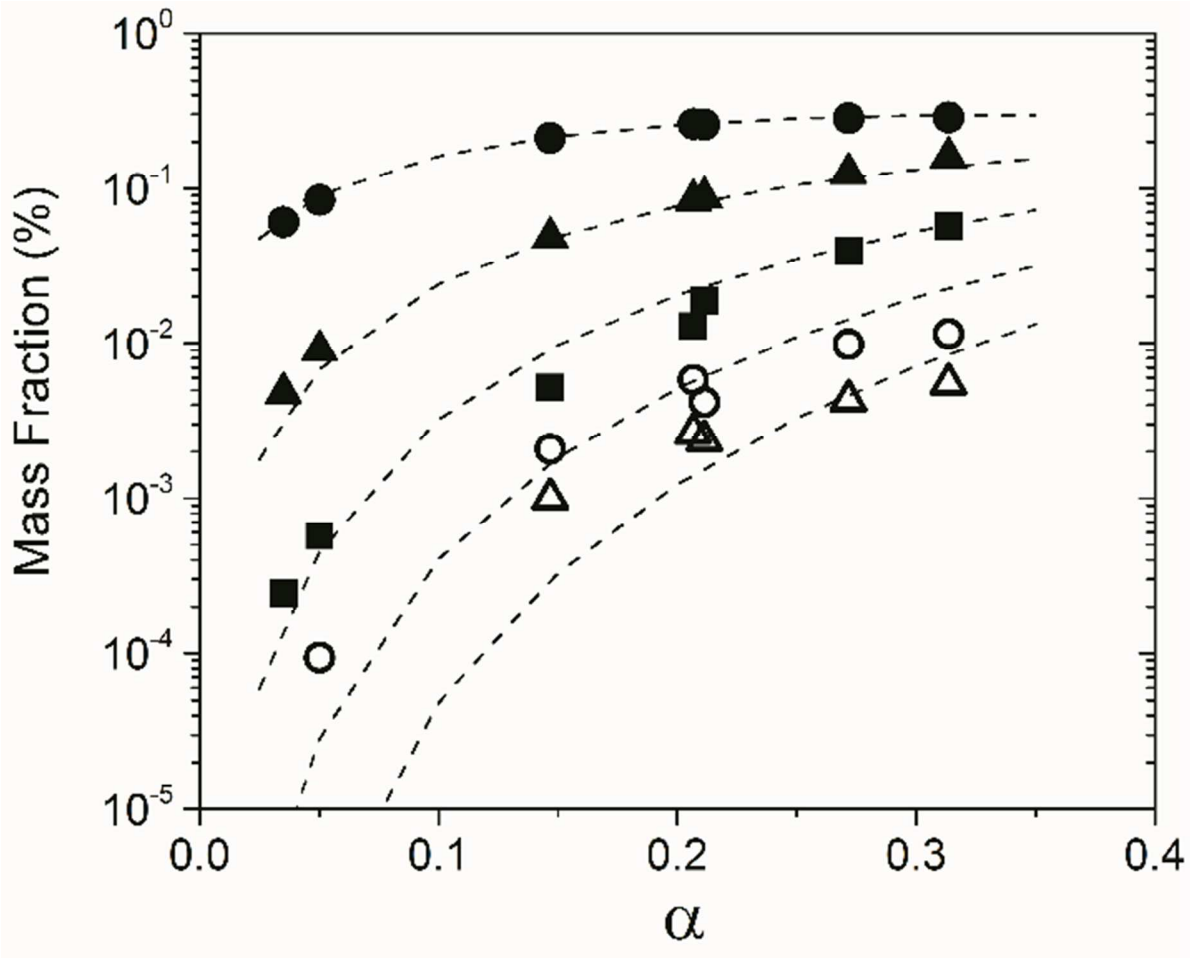

Figure 10. Mass fraction of alcohols-aldehydes with carbon number of C_4 (●), C_6 (▲), C_8 (■), C_{10} (○), and C_{12} (△) controlled by varying the residence time, during condensation reactions of ethanol-derived intermediates on Ca-HAP catalyst (5 kPa C_2H_5OH, 96 kPa H_2, 1.67 Ca/P, 573 K). Dashed lines are values predicted by the ideal step-growth model (Eq. (14)).[39,40]

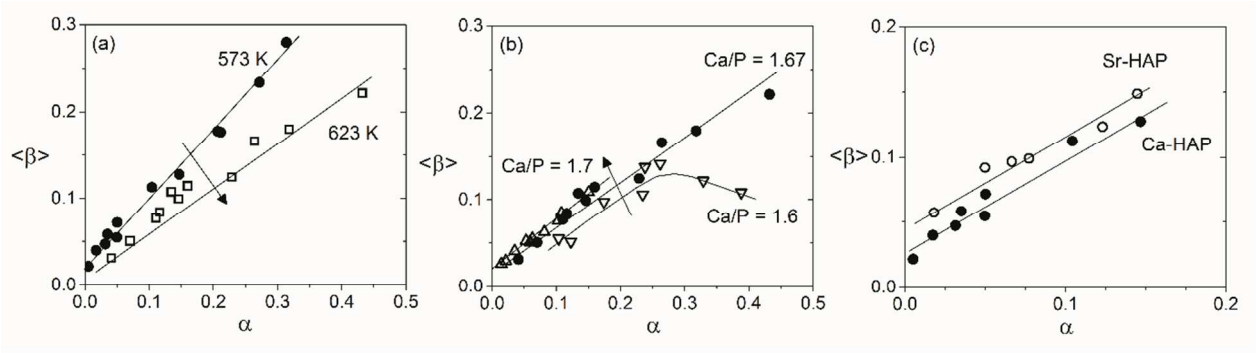

Figure 11. The change in the averaged branching factor of $C_{n>2}$ products during condensation reactions of ethanol-derived intermediates as functions of α, controlled by varying the residence time, on Ca-HAP materials (5 kPa C_2H_5OH, 96 kPa H_2, 573 K). (a) Effect of temperature (●, 573 K; □, 623 K, Ca-HAP (1.67)), (b) effect of Ca/P ratio (▽, 1.61; ●, 1.67; △, 1.74), and (c) effect of base sites (●, Ca-HAP (1.67); ○, Sr-HAP (1.71)). Solid lines in the figures are included to guide the eye.

Initial C–C Bond Formation Mechanism

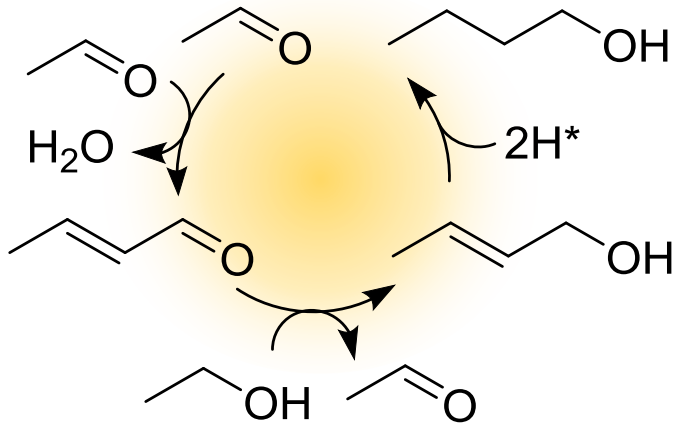

Product Distribution of Continuous Reaction

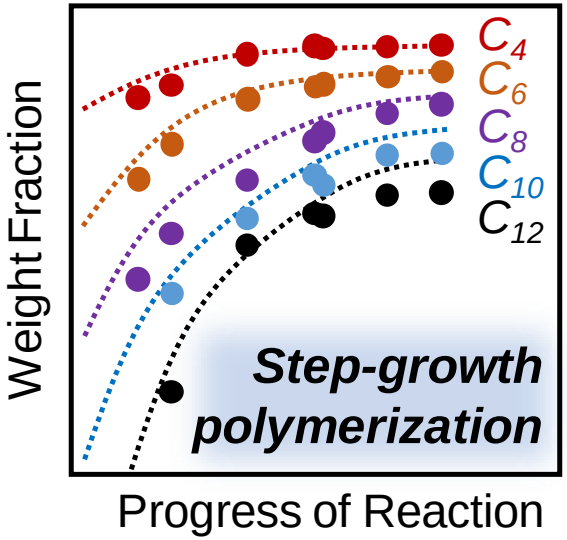

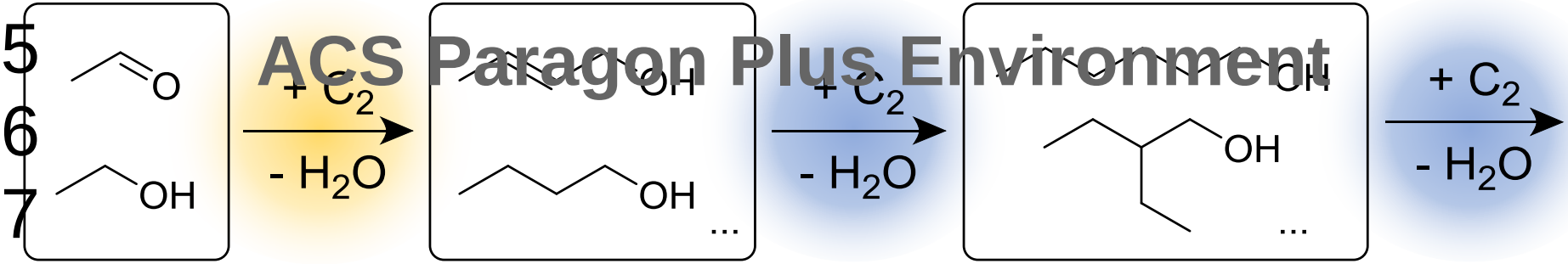

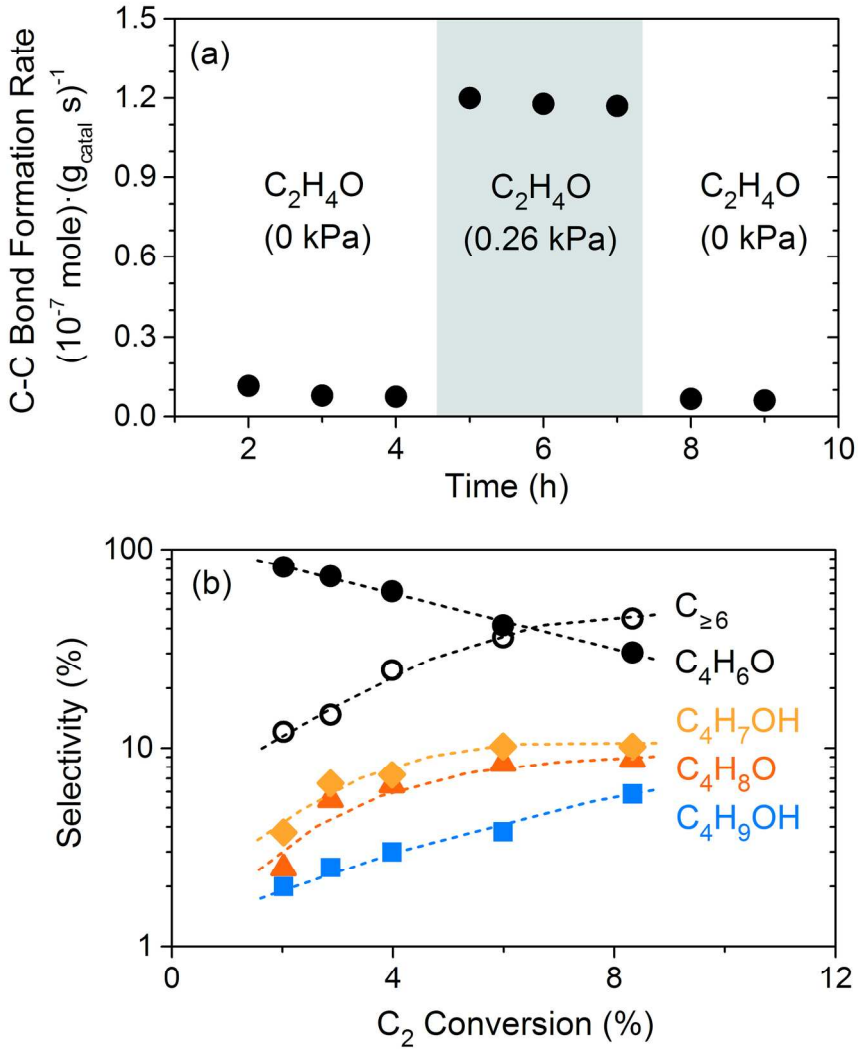

89x100mm (600 x 600 DPI)

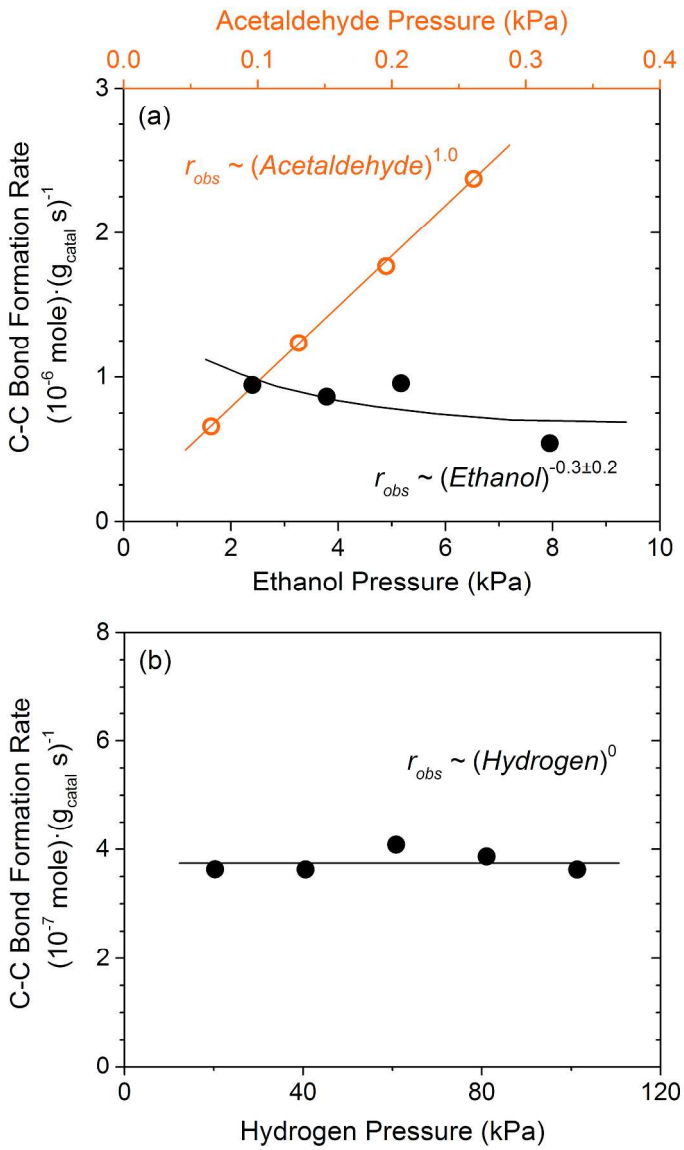

118x176mm (600 x 600 DPI)

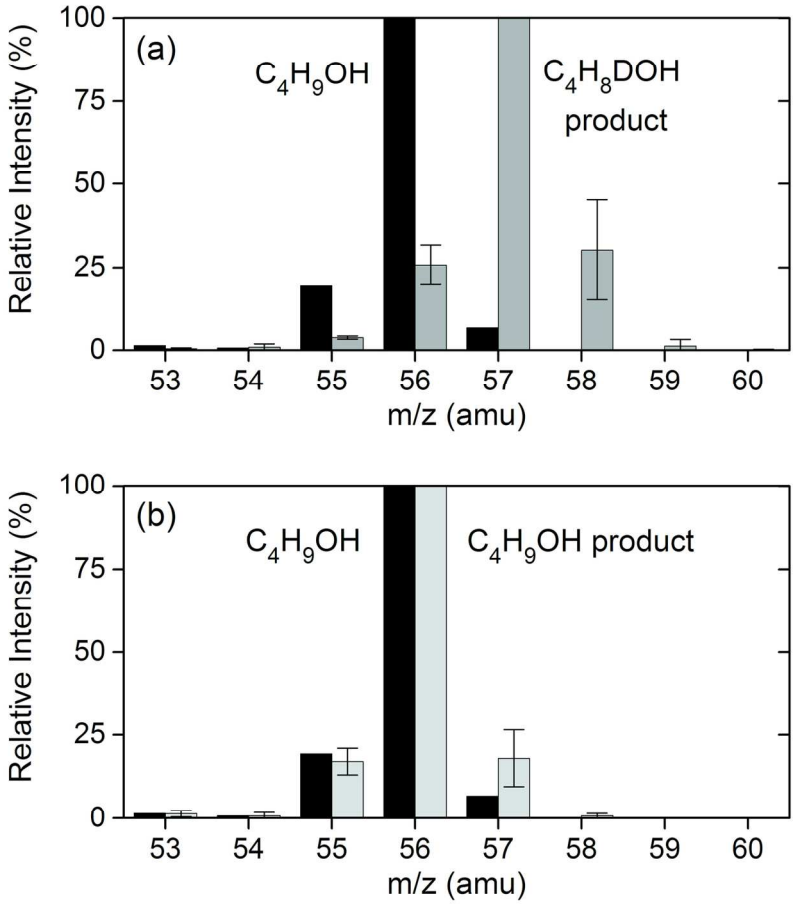

76x73mm (600 x 600 DPI)

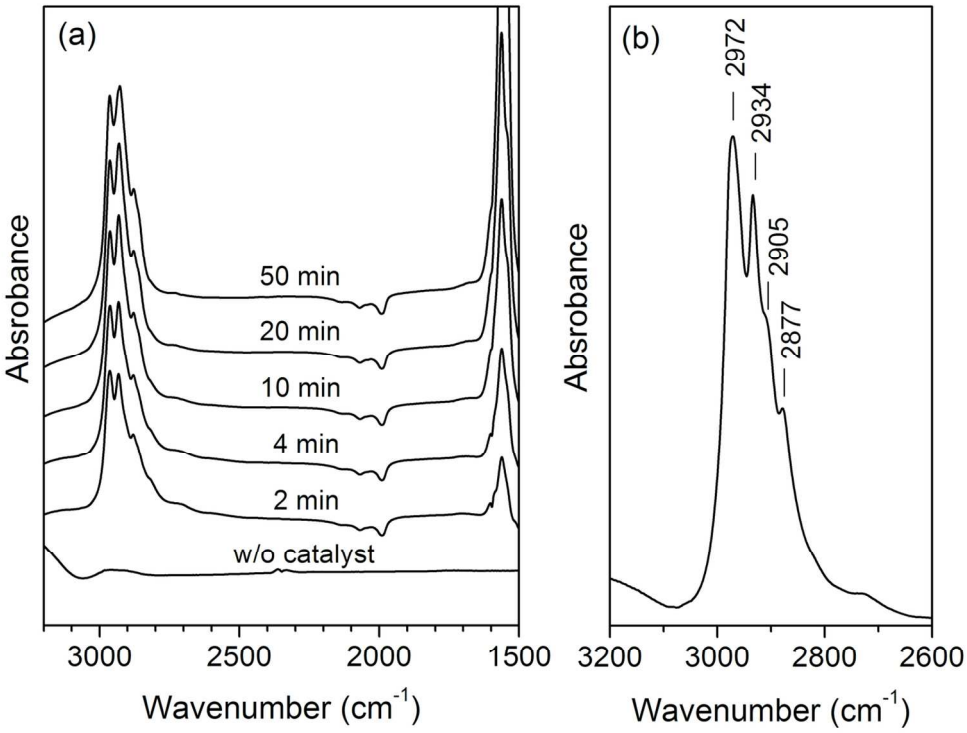

62x49mm (600 x 600 DPI)

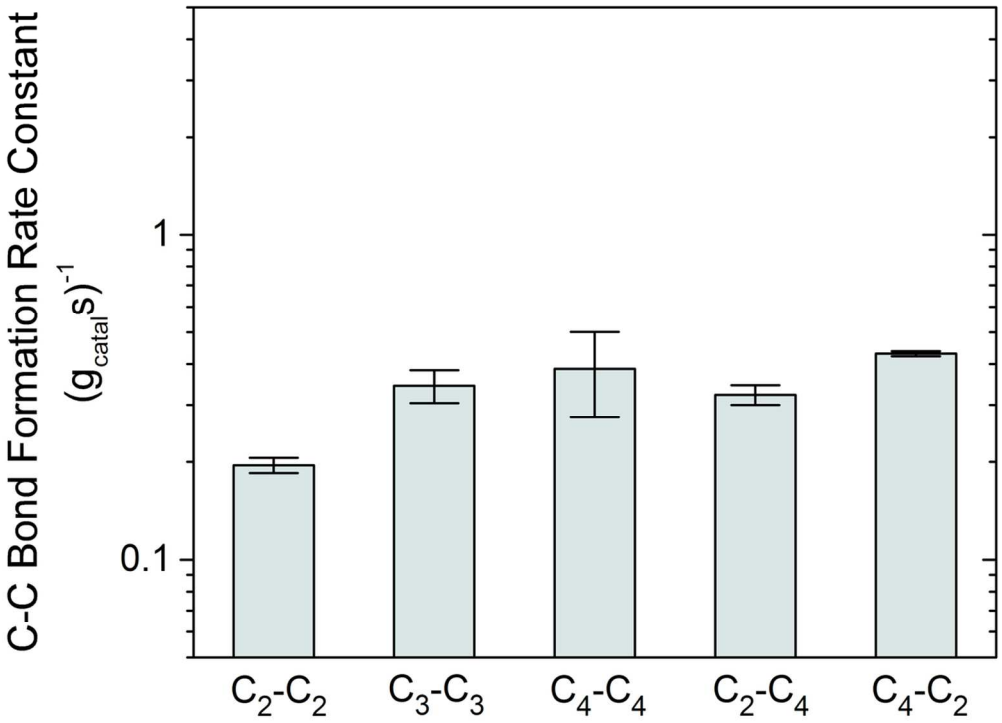

57x41mm (600 x 600 DPI)

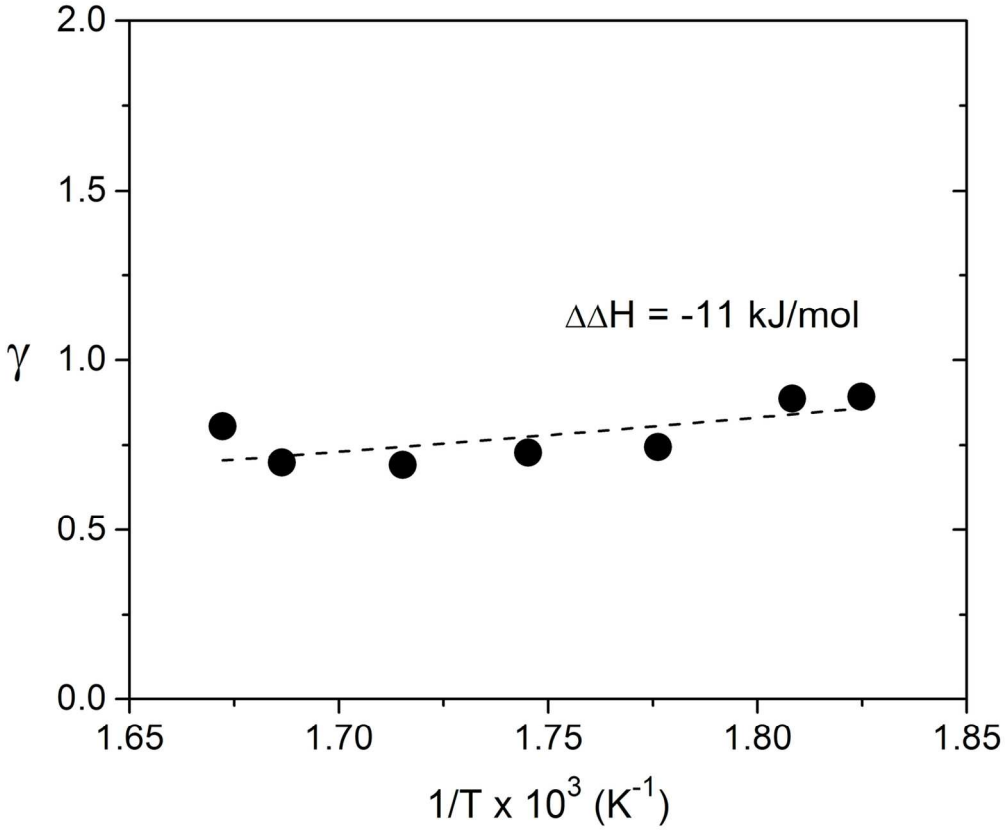

66x55mm (600 x 600 DPI)

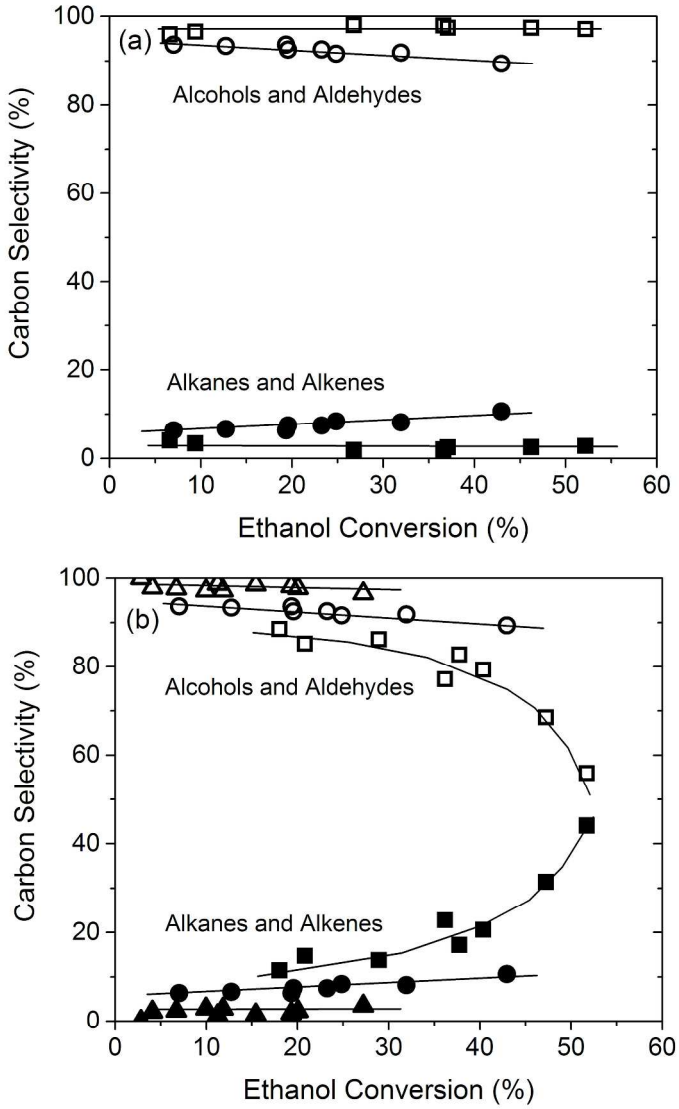

115x167mm (600 x 600 DPI)

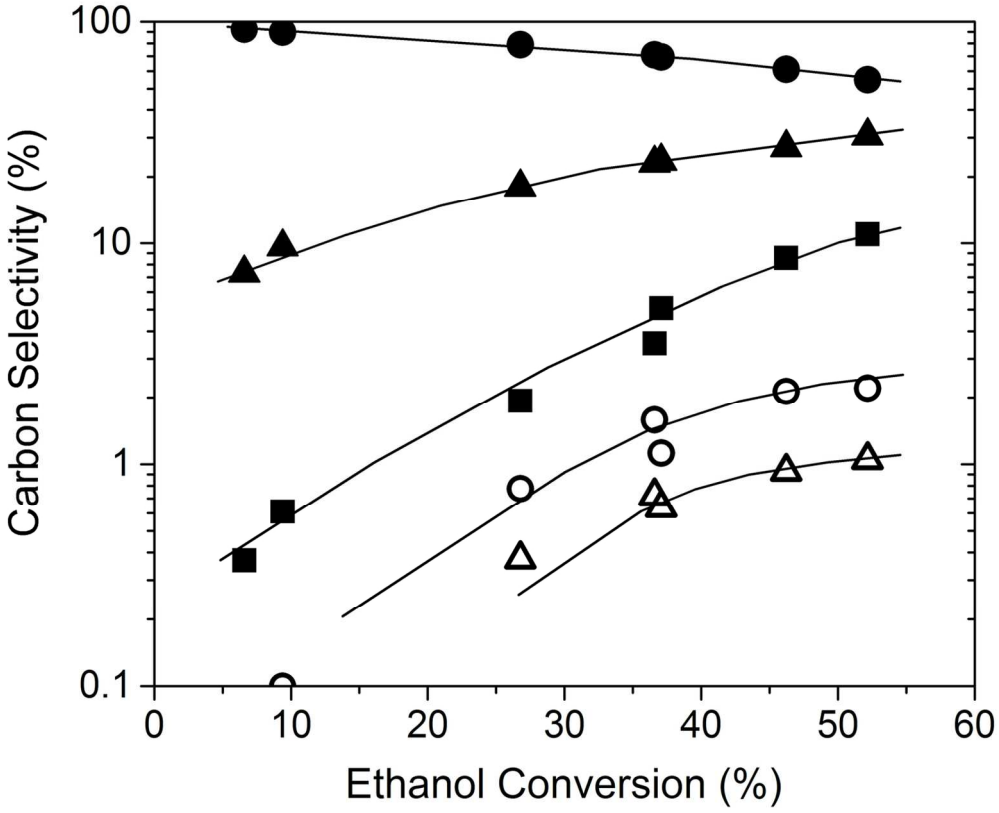

64x52mm (600 x 600 DPI)

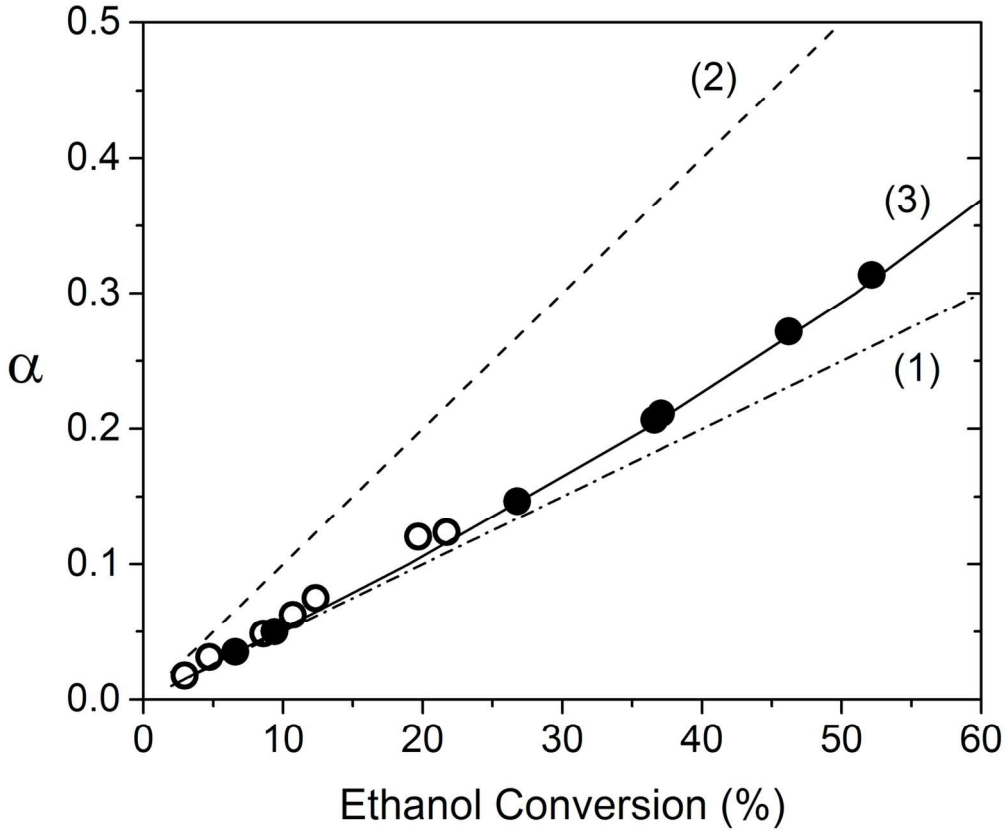

66x55mm (600 x 600 DPI)

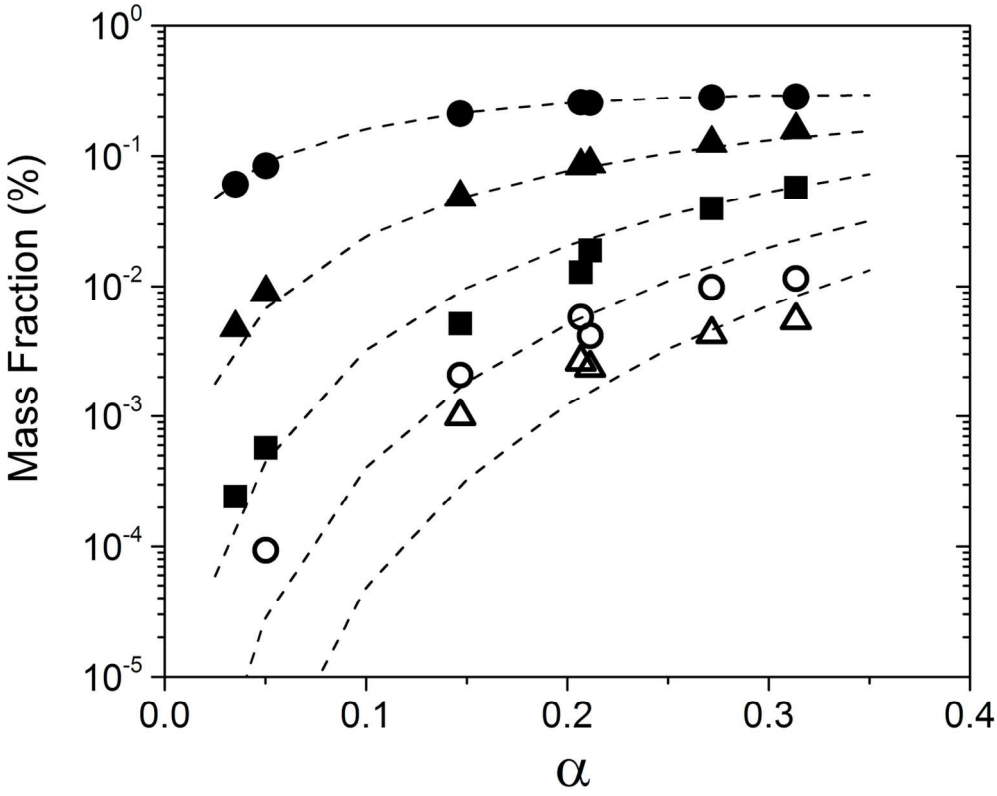

64x51mm (600 x 600 DPI)

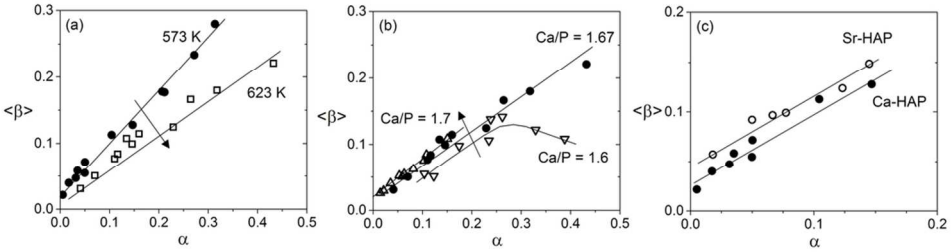

49x14mm (600 x 600 DPI)

$$C_2H_5OH + *_A \rightleftarrows C_2H_5OH*_A \quad (1.1)$$

$$C_2H_5OH*_A + *_B \rightleftharpoons C_2H_5O*_A + H*_B \quad (1.2)$$

$$C_2H_5O*_A + *_B \rightleftharpoons C_2H_4O*_A + H*_B \quad (1.3)$$

$$C_2H_4O + *_A \rightleftarrows C_2H_4O*_A \quad (1.4)$$

$$C_2H_4O*_A + *_B \rightarrow C_2H_3O*_A + H*_B \quad (1.5)$$

$$C_2H_3O*_A + C_2H_4O*_A \rightleftharpoons C_4H_7O_2*_A + *_A \quad (1.6)$$

$$C_4H_7O_2*_A + H*_B \rightleftharpoons C_4H_8O_2*_A + *_B \quad (1.7)$$

$$C_4H_8O_2*_A + *_A \rightleftharpoons C_4H_6O*_A + H_2O*_A \quad (1.8)$$

$$C_4H_6O*_A + C_2H_5OH*_A \rightleftharpoons C_4H_7OH*_A + C_2H_4O*_A \quad (1.9)$$

$$C_4H_7OH*_A + 2H*_B \rightleftharpoons C_4H_9OH*_A + 2*_B \quad (1.10)$$

$$C_4H_6O*_A \rightleftharpoons C_4H_6O + *_A \quad (1.11)$$

$$C_4H_7OH*_A \rightleftarrows C_4H_7OH + *_A \quad (1.12)$$

$$C_4H_9OH*_A \rightleftarrows C_4H_9OH + *_A \quad (1.13)$$

$$2H*_B \rightleftharpoons H_2 + 2*_B \quad (1.14)$$

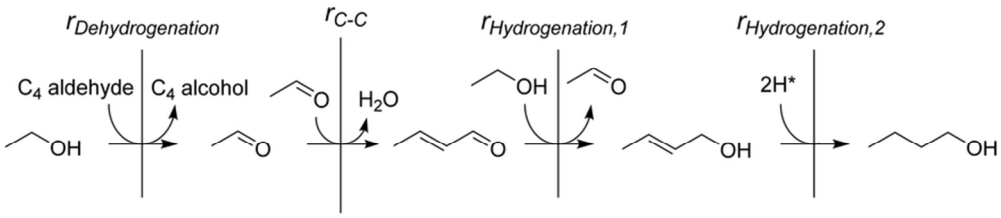

37x8mm (600 x 600 DPI)

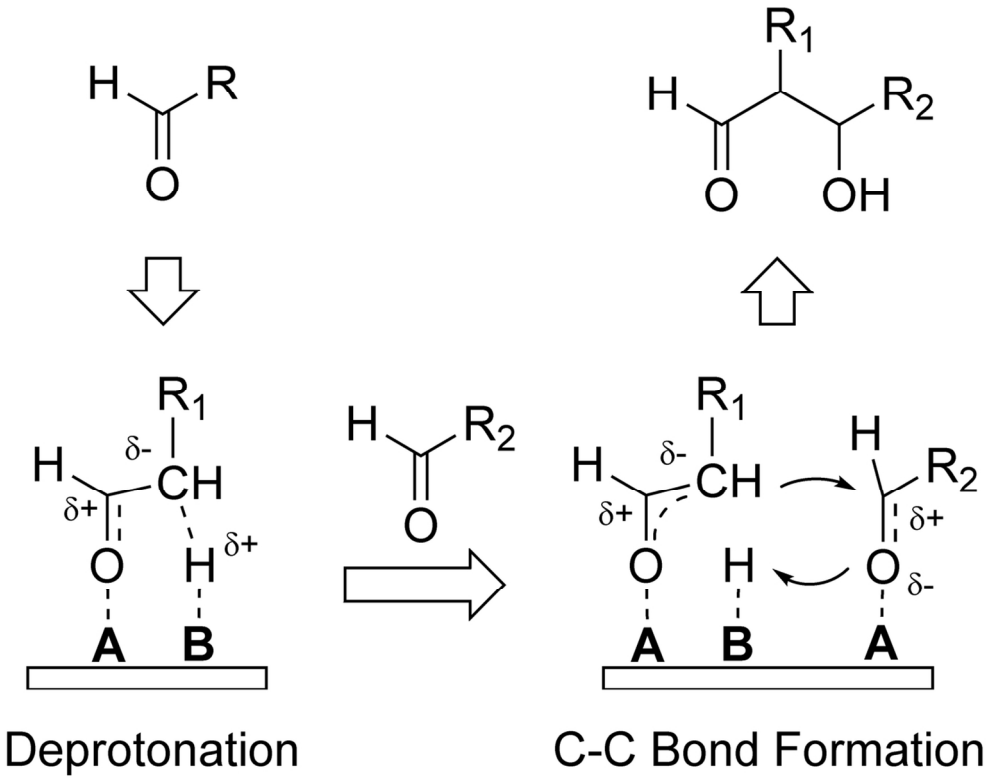

59x47mm (600 x 600 DPI)